MODE I FATIGUE AND FRACTURE OF THE CARBON FIBER REINFORCED POLYMER TO CONCRETE BONDED INTERFACE

by

Thomas Nicholas II

A dissertation submitted to the faculty of The University of North Carolina at Charlotte in partial fulfillment of the requirements for the degree of Doctor of Philosophy in Infrastructure and Environmental Systems

Charlotte

2010

Approved by:

_____

Dr. Shen-en Chen - Advisor

_____

Dr. David Young

_____

Dr. Anthony L. Brizendine

_____

Dr. Aixi Zhou

_____

Dr. Janos Gergely

_____

Dr. David Boyajian - Co-Advisor

ABSTRACT

Thomas Nicholas II. Mode I Fatigue and Fracture of the Carbon Fiber Reinforced Plastic to Concrete Bond Interface Region.
(Under the Direction of Dr. Shenen Chen and Dr. David M. Boyajian)

As wet, lay-up fiber reinforced polymers (FRP) continue to gain popularity in the redesign and retrofit of reinforced concrete structures; it becomes imperative to fully define the interaction between these materials. Until recently, the main body of FRP research focused on the flexural and shear strengths of the FRP to reinforced concrete system. However, in order to fully determine the capabilities of the structural system, the ability of the FRP to reinforced concrete bond to transfer the loads must be thoroughly investigated.

The preliminary research on defining the behavior of the FRP to concrete bond (deemed the interface in earlier studies) primarily used two types of testing methodologies, the double cantilever beam (DCCB) and the three point bending beam. Recently, the Single Contoured Cantilever Beam (SCCB) was proposed for materials that exhibit brittle failure and are weak in tension.

The overreaching goal of the current study is to better define the behavior of the bonded interface of reinforced concrete and carbon fiber reinforced polymers (CFRP). The study will utilize the surface profile 3 (SP 3) as the finished substrate surface and ascertain its effect on the system as it pertains to Mode I fracture and fatigue. The work is presented as three main contributions (journal articles) that address fracture of the concrete to CFRP bonded interface, an analytical model (FE) of the SCCB system, and fatigue of the concrete to CFRP bonded interface. A limited study on durability of the interface subjected to Mode I fatigue is also presented in Appendix B.

In Chapter 2, the fracture behavior of the bonded interface using the SP 3 surface profile is investigated. Nine specimens with varying compressive strengths were tested to failure. The analysis shows that the critical strain energy release rate is a function of both the compressive strength of concrete and the mix design. A comparison of the results to past works was utilized to validate the current study results.

The third chapter presents an analytical study (finite element) for fracture of the concrete to CFRP bonded interface. The model utilizes the ABAQUS® defined cohesive element to model the delamination of the interface. The results illustrate the ability of the cohesive element to effectively model the interface with a two percent difference in critical load between the model and the lab results.

The fourth chapter provides a foundational work on the fatigue life of the concrete to CFRP bond interface. For this objective, the SCCB was subjected to a cyclic loading of multiple loads for a load ratio of 0.5 and a frequency of five hertz. The results were then used to formulate a modified Paris Law equation for the prediction of fatigue life for the 0.5 load ratio and five hertz frequency. The resulting analysis provided the material constants of B and m as 2×10^{-8} and 3, respectively. Additionally, it was discovered that while shallower than fracture, the failure occurred predominantly in the substrate.

ACKNOWLEDGMENTS

They say it takes a village to raise a child, I feel as if it took the same for me to get to this point in my academic career. I would first like to thank my gracious committee, Dr. Chen, Dr. Young, Dr. Brizendine, Dr. Zhou, Dr. Gergely and Dr. Boyajian, for their never wavering commitment to my work. Your guidance has been invaluable and I count myself blessed to have studied under you. I would like to thank my advisors Dr. Chen and Dr. Boyajian; you have been mentors and friends throughout this process and I hope for many years to come. I would also like to thank Mr. Mike Moss, Mr. Dan Rowe and Mr. Bill Lindsey for their patience and assistance during my research. Finally to Dr. Brizendine, who started me on this merry-go-round so many years ago, I could not have done it without you. I will always appreciate what you have done for me and I promise to pay it forward.

Not often do we get to thank the ones who never ask of it and never need it, I would like to take this opportunity to thank my family. First, my dad, for teaching me that hard work and perseverance are qualities that lead to success. The greatest compliment I think I can pay you is that of all the things you have taught me, the one I cherish the most is how to be a good father to my son. To my brother, for keeping me grounded during this process and for your support, it went farther than you know. To my mother, my only regret is that you will not be there when I finally finish. I miss you and I hope wherever you are, you are proud of your son.

Finally, I must thank the two most important people in my life, my wife, Melissa and my son, Ty. I'm not sure I can express what you have meant to me during this

process. You have supported me through every crazy idea, ups/downs, late nights and early mornings. You are my rock. I love you and I dedicate this work to you.

TABLE OF CONTENTS

LIST OF TABLES

LIST OF FIGURES

CHAPTER 1: INTRODUCTION

1.1 Overview

As the reinforced concrete infrastructure continues to deteriorate, the engineering community is turning to rehabilitative methods as cost effective alternatives to replacement. One such method that has gained popularity over the last few decades, is the use of wet-layup fiber reinforced polymers (FRP) adhered to the concrete surface. The application of FRP consists of a fibrous material (carbon, glass, Kevlar) that has been impregnated by an epoxy material which is then bonded to the surface of the reinforced concrete structure. Standards for the application of FRP to a concrete surface are provided by ACI 440.2R-08 (ACI, 2008). As the popularity of FRP applications has risen, so has the research into the material's behavior. Until recently, the bond behavior of the FRP to concrete interface had not been rigorously evaluated as it pertained to Mode I (opening) failure due to limitations in testing low tensile capacity bonded materials.

A number of methodologies have been presented recently in various papers that quantifies the mode I failure of the reinforced concrete to FRP bonded interface. Qiao and Xu (2003) presented a modified three point bending beam to measure the mode I fracture energy of the bonded interface region with good results. Additionally, Giurgiutiu et al (1999) presented a modified double cantilever beam that performed well for determining mode I failure. However, as with most bonded interface test methodologies,

the crack tip location must be physically measured during the test. This presents a difficult task as the exact location of the crack tip is visually challenging and cumbersome. Furthermore, existing large scale tests for strength and stiffness evaluations do not detect delamination effects, while small scale tests only provide average interface strength properties that neither describe failure mechanisms nor provide fracture toughness data. In 2002, Boyajian et al. presented the Single Contour Cantilever Beam that provided a testing methodology which negated the need to measure the crack tip location and overcome large- and small-scale test shortcomings.

With the advent of the Single Contour Cantilever Beam (SCCB) testing methodology, the limitations of the Double Cantilever Beam (DCB) test methodology are easily overcome. In determining fracture toughness, the SCCB relies on an optimized contour shape determined by multiple finite element analyzes and further refined during experimental calibrations. The experimental calibrations are currently necessary due to fixity limitations, or hinging action, of the wood contour. For these reasons and the adaptability for the fatigue tests, the SCCB was chosen for this study.

1.2 Problem Statement and Objectives

The overreaching goal of the current study is to better define the behavior of the bonded interface of reinforced concrete and carbon fiber reinforced polymers (CFRP). The previous work by Lawrence and Boyajian (2006), Kodkani (2004) and Boyajian (2002) has provided a solid foundational work on developing and utilizing the SCCB to effectively quantify the behavior of the CFRP to reinforced concrete bond interface. As complete as the previous work has been, a number of gaps remain to fully understand the

bonded interface behavior. The current effort focuses on four main areas of concern that have not been previously discussed in depth: the effect of the compressive strength of concrete on the critical strain energy release rate; the effect of the International Concrete Repair Institute surface preparation 3 (SP 3) on the critical strain energy; development of an analytical model for the SCCB; and the behavior of the bonded interface region that experiences a cyclic load. The specific objectives of this research were:

1. Determine the behavior of the concrete to CFRP bonded interface that has been prepared to the ICRI surface profile level three as a function of the 28-day compressive strength of concrete. Using target concrete compressive strengths of 27.58 MPa, 34.50 MPa, and 41.40 MPa, four SCCB specimens for each target compressive strength were tested to fracture.
2. Develop a finite element analysis model utilizing a damage evolution model that effectively predicts the critical strain energy release rate of the bonded interface. The model will utilize the ABAQUS® defined, cohesive element to model the interface region. The model will then be analyzed based on different concrete compressive strengths of the substrate and compared to the laboratory tests.
3. Determine the fatigue life of the bonded interface that has been subjected to a frequency of five hertz and a load ratio of 0.5. For the foundational work of fatigue of the bonded interface using the SCCB, four SCCB specimens will be used to develop the fatigue life of the bond by developing the modified Paris Law. The frequency of five hertz was selected due to most engineering structures experience frequencies of one to five hertz over a 120 year life span

(Ferrier et al, 2005). According to Zhang and Wu (1997), a frequency of one hertz is referred to as a low fatigue life and five hertz is labeled as middle fatigue life. While load ratio will have an effect on the fatigue life of the bonded interface, $R = 0.5$, was selected to provide mid level values (e.g. R: 0 → 1).

1.3 Organization

The dissertation is a compilation of three scholarly papers, in which, each are presented as a chapter in this document as well as work performed on the durability of the SP 3 surface preparation (Appendix B). Each paper is comprised of an abbreviated literature review, research methodology and data, test results, conclusions, and references. The final chapter of the dissertation represents summarized conclusions of each of the papers and provides direction for future research on the bonded interface.

1. The first paper presents the findings from the critical strain energy release rate of the bonded interface where the reinforced concrete substrate surface was treated to the ICRI surface profile level three (SP 3). Additionally, the 28-day concrete compressive strength was varied to investigate its effect on the critical strain energy release rate. As with all physical laboratory tests in this study, the SCCB testing methodology was utilized to determine the bonded interface fracture toughness.
2. The second paper utilizes the commercially available finite element software ABAQUS® to analytically determine the critical energy release rate of the bonded interface. For this finite element model, the bonded interface was modeled using the cohesive element, otherwise known as a damage evolution

element. The finite element model results were compared to the laboratory test results.

3. The third paper provides a foundational work on the fatigue life of the concrete to CFRP bond interface. For this objective, the SCCB was subjected to a cyclic loading of multiple loads for a load ratio of 0.5 and a frequency of five hertz. The results were then used to formulate a modified Paris Law equation for the prediction of fatigue life for the 0.5 load ratio and five hertz frequency.

The appendices consist of five sections. Appendix A contains material data as well as the specimen inventory. Appendix B presents the preliminary work on Mode I fatigue and durability of the bonded interface. Appendix C provides the abbreviated FEA fracture model input data. Appendix D presents miscellaneous photos of specimens not presented in the body of the dissertation.

CHAPTER 2: MODE I FRACTURE OF THE REINFORCED CONCRETE TO CFRP BOND INTERFACE UTILIZING THE ICRI SURFACE PROFILE THREE

Submitted to the *Journal of Composites for Construction*

Thomas Nicholas, UNCC and David M. Boyajian, Taylor University

MODE I FRACTURE OF THE CFRP-REINFORCED CONCRETE BONDED INTERFACE REGION UTILIZING INTERNATIONAL CONCRETE REPAIR INSTITUTE (ICRI) SURFACE PROFILE PREPERATION STANDARDS

ABSTRACT

As the reinforced concrete infrastructure continues to decline, the engineering community is turning to rehabilitative methods as cost effective alternatives to replacement. One such method, that has gained popularity over the last few decades, is the use of wet-layup fiber reinforced polymers (FRP) adhered to the concrete surface. The application of FRP consists of a fibrous material, which when impregnated by an epoxy, may then be bonded to the surface of a reinforced concrete structure. Standards for the application of FRP-to-concrete surfaces are provided by ACI 440.2R-08 (ACI, 2008). The experimental fracture mechanics approach known as the Single Contoured-Cantilever Beam (SCCB) was herein utilized to determine the Mode I critical strain energy release rates of the carbon fiber reinforced polymer (CFRP) variety of FRPs as reinforcement to the underlying concrete members. This study examines the effect of utilizing the ICRI surface preparation standards on the concrete substrate and compares the work to a previous SCCB study. The results will illustrate that the critical strain energy of the concrete is a function of the compressive strength of the concrete and that the surface profile 3 (SP 3) surface profile produces a fracture that deeply penetrates the concrete substrate.

KEYWORDS: concrete repair; concrete strengthening; fiber reinforced polymer; surface roughness; fracture

Introduction

Since FRP-concrete bonded structures are only as good as the integrity of the composite media being bonded to the concrete substrate, this research seeks to investigate the strength of the interface through the opening, or Mode I, course of fracture failure. In order to accomplish this, it is important to first understand how the system in question fails. The interface region of an FRP-concrete bonded system is composed of the concrete substrate, the external fiber reinforcement lamina (or laminate), and the epoxy bonding agent, or adhesive, between these two to affix the latter media to that of the former. While there has been ample research on the fracture of FRP to concrete bonded interfaces (see Huang and Lyons (2005), Jia et al (2005), Karbhari (2000), Boyajian et al (2000), and Qiao and Xu (2004)) few have purposely used the surface profile 3 (SP 3) as directed by International Concrete Repair Institute (ICRI) and a number of manufacturers. The goal of this work is to experimentally quantify the behavior of carbon fiber reinforced polymer (CFRP)-to-concrete bonded interfaces in which the latter substrate media has been treated in accordance to the SP 3 graded level. Additionally, this study will determine what effect the substrate compressive strength has on the bond strength.

The failure of a bonded (adhesive) system can be described as stable or unstable cracking (Mostovoy and Ripling, 1975). In stable failures, the crack initiates once the critical load is reached and then extends at a constant strain energy. However, for unstable failures, the crack is propagated by reaching a critical load, arresting, and then reaching a critical load once again. As noted by Boyajian (2002), in actuality, most materials exhibit both types of cracking. In an effort to better describe the cracking

behavior of adhesive systems, River (2002) categorized four types of possible adhesive failures as strong/unstable, strong/stable, strong/moderately unstable and weak/stable with the preferable mode of failure being strong/stable. This crack-growth pattern is the product of a strong/tough adhesive used in conjunction with a tough substrate. The crack propagation for this category can occur into the substrate and therefore the fracture toughness can be a function of the substrate's fracture toughness. However, in most instances of this study, failures were found to be strong/moderately unstable.

The crack-growth for the strong/moderately unstable category occurs when the adhesive is stronger/tougher than the substrate. The crack propagation is primarily (or even totally) constrained in the substrate. Therefore, the fracture energy of the joint can be defined as the fracture energy of the substrate material. Once the critical load is reached the crack will arrest, allowing the fracture energy to again increase to critical levels.

Fracture behavior can normally be characterized as beginning with crack-initiation and intensifying through crack propagation. At the onset of crack initiation, the crack propagation behavior becomes a function of the displacement of the failed interface surfaces (Boresi et al., 1993). Irwin (1958) defined three failure modes to describe how the surfaces are displaced, denoted by fractures exhibiting Mode I, Mode II and/or Mode III cracking. Mode I describes a failure of the interface bond that occurs normal to the failed surface, often referred to as the opening mode. It should be noted that for most engineering situations the majority of fracture failures are intiated by Mode I failure (Hertzberg, 1976) and therefore is the focus of the current research. Mode II fracture can be characterized as shear normal to the fracture surface, in that, the surfaces slide (shear)

over one another, while Mode III represents a tearing failure. While most fractures can be described by one of the failure modes predominantly, the mixing of mode failures, such as the Mode I – Mode II interactions, is also commonly discussed.

The ability of an engineering material to resist these failure modes is frequently referred to as fracture toughness. The commonly accepted method for representing fracture toughness is the critical release strain energy, G_C, as defined by the Irwin-Kies (1954) equation:

$$G_C = \left(\frac{P_C^{\,2}}{2b} \right) \left(\frac{\mathrm{d}C}{\mathrm{d}a} \right) \tag{2-1}$$

Where:

G_C = Critical strain energy release rate, lbs/in (J/m^2)

P_C = Critical load, lbs (N)

b = width of the specimen, in (mm)

dC/da = Rate of compliance (C) with respect to crack length (a), lbs^{-1} (N^{-1})

It should be noted, the critical strain energy release rate, G_C, will be denoted as G_{Ic} herein to distinguish it as being due to Mode I failure. For an in depth derivation of the Irwin-Kies equation, the reader is directed to review Irwin and Kies (1954), Carlsson and Pipes (1987), Polakowski and Ripling (1966), Bazant and Planas (1998) and Boyajian (2002).

Compliance

In employing the SCCB testing methodology (Boyajian, 2002), the success of determining the critical strain energy release rate is directly related to the accuracy of

compliance. As first presented in the Irwin-Kies equation, compliance, C, is represented by a ratio of displacement to load increment and can also be represented as the inverse stiffness of the structural element. For the SCCB, the accuracy of compliance becomes a function of the accuracy of the contour (see Figure 2.1 for contour dimensions). In the absence of a contoured cantilever, the compliance of the un-contoured beam changes as the crack location, a, propagates along the structural member. As a result, calculating the critical strain release energy can only be achieved by continuously measuring the crack location during the experiment which is a difficult task. As a means to avoid the arduous measuring of crack tip location, a contoured shape is utilized that causes the compliance to change linearly in conjunction with crack propagation along the interface (Boyajian, 2002). This linear relationship removes the dependence of load, P, and strain energy release rate, G_I, from the crack tip location, a.

In determining the optimized contour dimensions and in an effort to simplify the procedure, the dimensions of the contour are prescribed prior to analysis, except for, h_f (the height of the contour given in Figure 2.2 as 95 mm, which will be iterated in a finite element model (FE) to achieve several approximated contour shapes. The crack tip location begins at 51 mm (starter crack) loaded with 448 N and the corresponding contour deformation at the load location is recorded. The process is repeated for crack tip locations at 51 mm intervals up to 357 mm of specimen length. The resulting compliance, C (calculated as u/P), is plotted as a function of crack tip location, a. The slope of the linear relationship provides the compliance gradient, dC/da. Subsequently, for each h_f that yields acceptable compliance gradients, an experimental calibration must be performed to assist in the final optimization of the contour.

This study utilized the previously calibrated contour developed by Lawrence and Boyajian (2006) which had an h_f = 95 mm. The contour was modeled in ANSYS® in an effort to check the compliance gradient. The result of the analysis is illustrated by Figure 2.1 where compliance is plotted as a function of each crack tip location, a. The resulting gradient used for the fracture studies was $dC/da = 1.49\times 10^{-5}$ N^{-1} which compares well with Boyajian (2002).

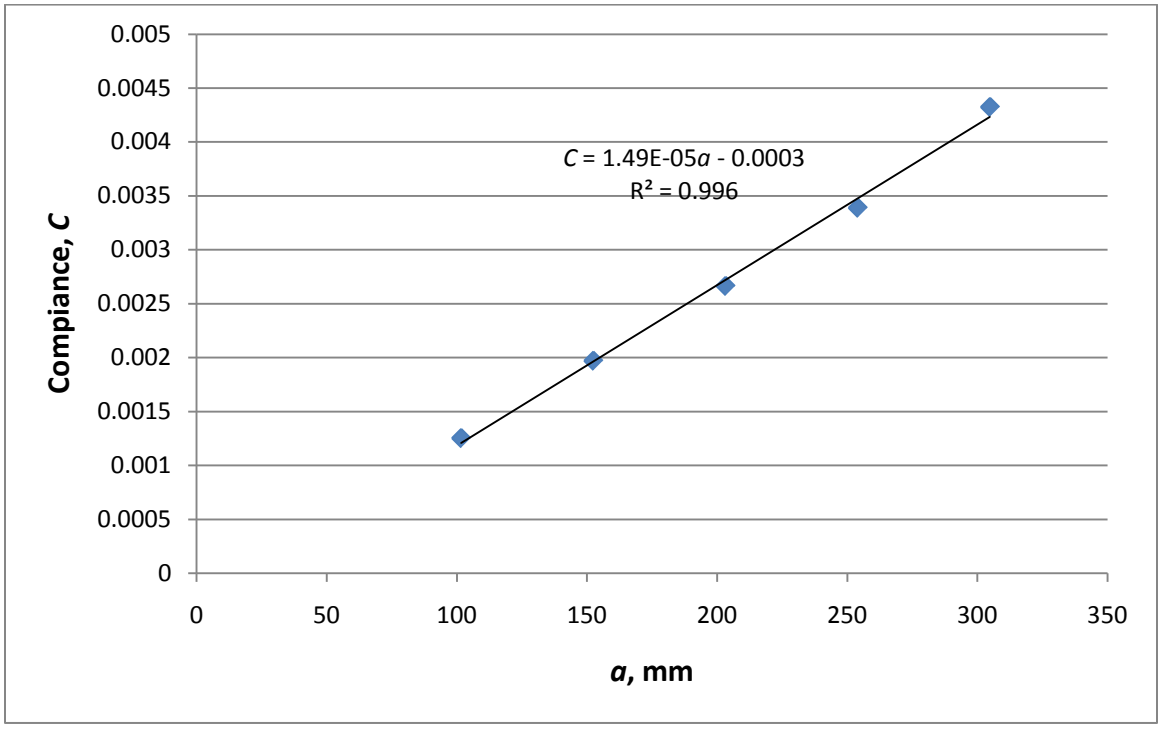

Figure 2.1. Compliance Gradient of the 18" (457 mm) Contour

Materials

The SCCB used for this study is composed of a substrate material (reinforced concrete), a fiber reinforced composite layer (CFRP, in this case), and a wood contour as illustrated in Figure 2.2, as representative of the SCCB used by Boyajian and Lawrence, in that the beam length dimension is equivalent. The dimensions for the substrate beam will be further discussed in the following section. Referring to previous SCCB studies,

Kodkani, Davalos, and Boyajian, utilized SCCB specimens that were 483 mm and 686 mm long. While not addressed specifically in this paper, the behavior of the debonding is not a function of bond length and therefore, the results of the fracture testing should be consistent with the previous studies.

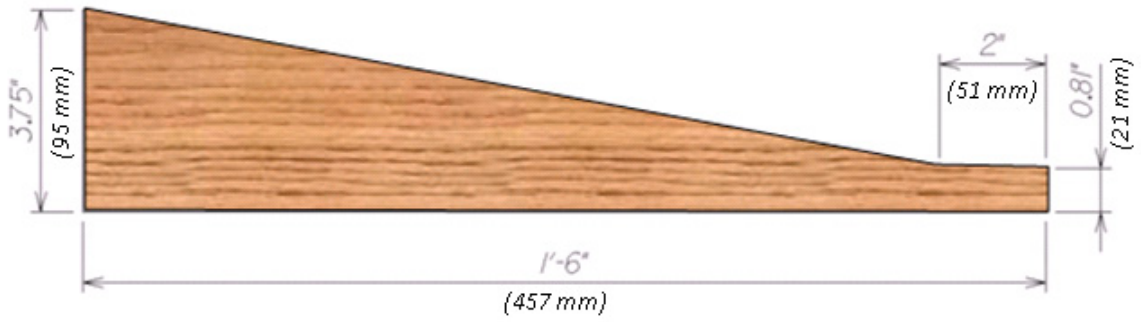

Figure 2.2 Single Contour Cantilever Beam

Concrete Mix Design

As previously stated, the bonding substrate for the system is a reinforced concrete beam illustrated by Figure 2.3. The target ranges for the concrete compressive strength was 27.58 ± 1.73 MPa, 34.50 ± 1.73 MPa and 41.40 ± 1.73 MPa among batches for consistency and comparison to previous work. The only derivation in testing protocol from previous studies was the mix design. The previous studies (Lawrence and Boyajian (2005), Kodkani (2004)) utilized approximately 1:1:1 and 1:2:4 ratios as the mix designs so as to increase the workability of the concrete into the mold and produce a consistent concrete surface. For the current work, the mix design was found using ACI 301 (2005) mix specifications which produced the more commonly used 1:3:5 mix design. While the issues of workability and a constant concrete surface are still true for the current study,

they were addressed by employing a vibration table to fill voids and work the concrete into the mold. Additionally, a slump of 89 mm was used to further aid in workability.

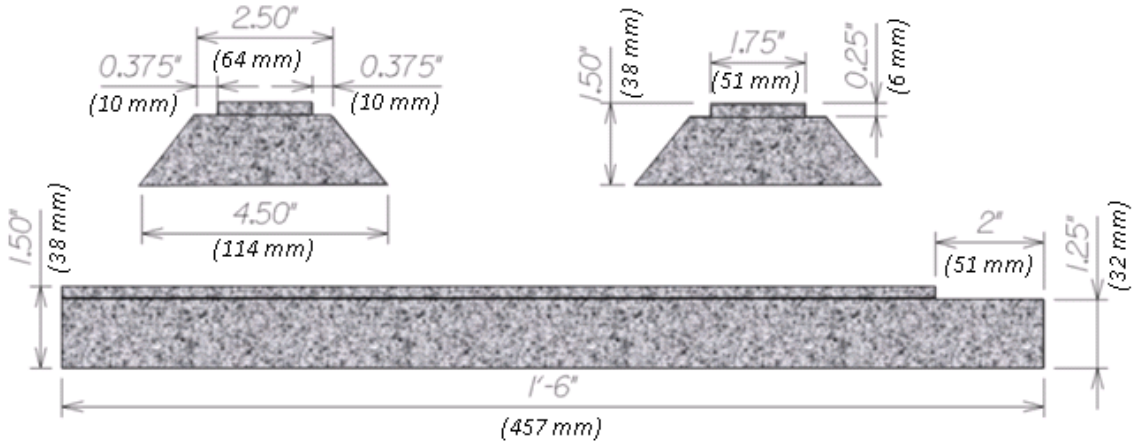

Figure 2.3 Concrete Beam Dimensions

The only additive used in the mix design was an air entrainment agent which was added to achieve 6.5 percent ± 1 percent average air content. The addition of an air entrainment agent was necessary due to future durability testing.

The testing regimen used by the entire study required a total of 62 concrete beam specimens; however, only 9 of the 62 were required for this effort. Ideally, all 62 beams would be poured at the same time from the same batch; however, the total number of specimens was limited to 18 per batch due to form constraints, resulting in four separate pours. For each batching, the concrete was tested for slump, air entrainment, and compressive strength. The batch was considered successful if it met the mix design requirements defined in the previous section. The average compressive strengths among the batches were 28.96 MPa (SD =2.34 MPa), 36.89 MPa (SD =0.10 MPa) and 40.85 MPa (SD =0.10 MPa) with all batches meeting the compressive strength standards. Additionally, the air content and slump averages met the required project standards.

Fiber Reinforced Polymer System

The fiber reinforced polymer used in the study consists of two parts: the carbon fibers and epoxy. The system selected for the study was Sikadur® 301 two-part epoxy and SikaWrap® Hex 103C carbon fiber due to the system's increasing popularity in industry. The higher demand for the Sika 301 epoxy is a result of a lower cost for material and the lack of a primer coat, which in turn allows for faster construction times. The material properties for the system are listed in Table 2.1.

Table 2.1 Fiber Reinforced Polymer Properties (Sika®)

	SikaWrap® Hex 103C	Sikadur® 301
Tensile Strength	3.793 GPa	52.0 MPa
Tensile Modulus	234.5 GPa	2.000 GPa
Elongation	1.5 %	3.5 % @ break

Microllam® Laminated Veneer Lumber

The contour material used in the study is a wood product, 1.9E Microllam® LVL (Laminated Veneer Lumber) manufactured by Weyerhaeuser. The material was selected to serve as the contoured member of the SCCB specimen due to the ease by which it could be shaped as required by the compliance results (refer back to Fig. 3.1). The material properties are listed in Table 2.2.

Table 2.2 1.9E Microllam® LVL Properties

Grade	G Shear Modulus of Elasticity	E Modulus of Elasticity	E_{min} Adjusted Modulus of Elasticity	F_b Flexural Stress
1.9E	819 MPa	13 GPa	6.6 GPa	18 MPa

Substrate Surface Preparation

A significant deviation of the current study from previous work is the level of surface preparation. The International Concrete Rehabilitation Institute (ICRI), the American Concrete Insitute (ACI), and Sika®, mandates a minimum surface profile level 3 (SP 3) when adhering the wet layup of FRP as bonded to concrete surfaces (ICRI, 2003). Lawrence and Boyajian (2006) investigated the effects of bond strength as a function of surface profiles for surfaces that were virgin, grinded and sandblasted. The study, illustrated in Figure 2.4 showed that the rougher surfaces (sand blasted) produced a stronger bond; however, the surface profile of the sand blasted concrete in that study would only be classified primarily as a SP 2.

In order to achieve the necessary surface profile, the ICRI standards allows for shot blasting, sand blasting or pressurized water to be used. After numerous trials, the surface preparation method that produced the most consistent results was pressurized water from a 34.47 MPa pressure washer. Additionally, a set of surface profile tabs were obtained to assist in classifying the surface. The surface profile tabs are raised surface, rubber square swatches which illustrate each of the ICRI surface profiles. The common method for classifying the surface is to check the target surface tab (SP 3), as well as, the

tab above (SP 4) and the tab below (SP 2). Figure 2.5 illustrates a virgin concrete surface compared to a surface that has been treated to SP 3 specifications.

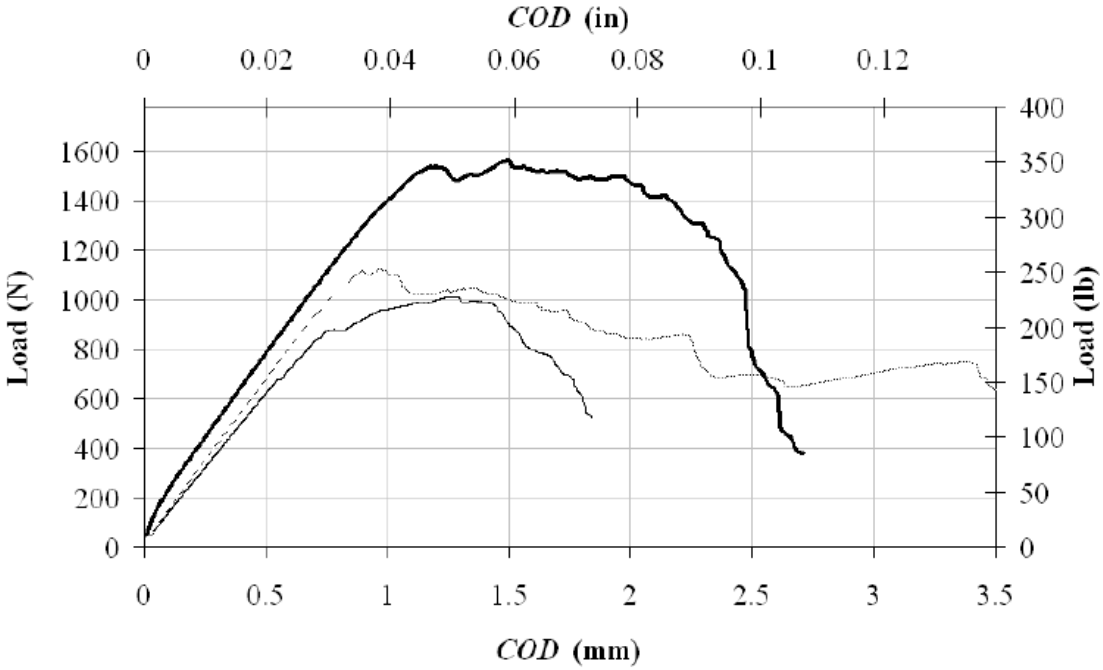

Figure 2.4 CFRP SCCB Test Results for Different Surfaces – Dark Black Line is SP 2 Surface, Medium Black Line is Mold Surface. (Lawrence and Boyajian, 2006)

Figure 2.5 Comparison of Virgin Concrete Substrate (Center) and SP 1 Substrate (Left) and SP 3 Substrate (Right)

Fracture Results

The SCCB previously described in Section 1 of this study was used to investigate the fracture behavior of the SP 3 bond interface. The testing regimen, as it pertains to fracture, was consistent with those of previous studies as presented in this section. The SCCB specimens were placed in the Instron 5582® machine and loaded until complete interface fracture ensued. An illustration of the test is presented in Figure 2.6.

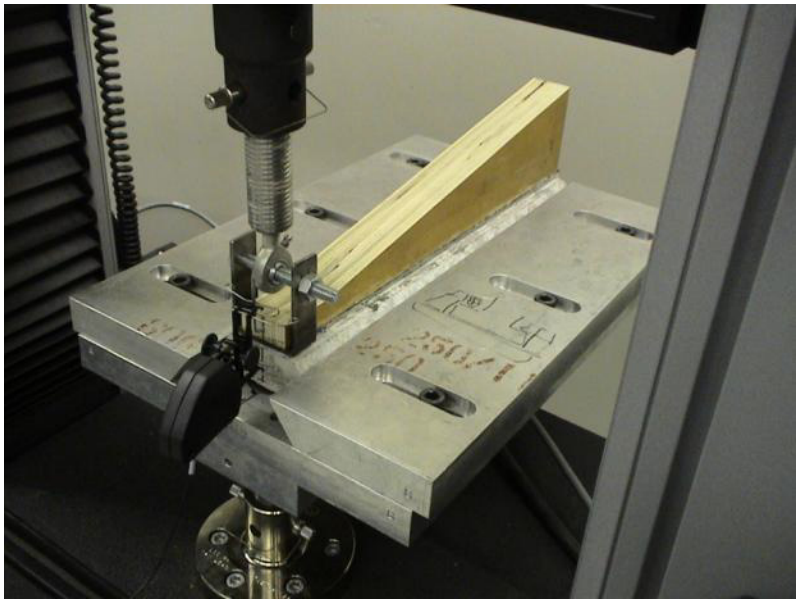

Figure 2.6 Single Cantilever Contour Beam Fracture Test in Instron 5582® (Lawrence and Boyajian, 2006)

A total of nine specimens were fractured for collection of preliminary data, utilizing different concrete strengths and CFRP applications. As listed in Table 2.3, FRAC27_T and FRAC27_D developed higher critical strain energies. These specimens utilized a substrate with a compressive strength of 40.85 MPa and the SP 3 surface profile.

The difference between the two specimens was the CFRP application process. For FRAC27_T, the CFRP was impregnated and applied utilizing a forceful application (squeegee and roller). On the other hand, for the FRAC27_D specimen, the CFRP was impregnated and applied under lighter forces (paint brush/squeegee). As can be seen in Figure 2.7, the fracture energy represents a strong/moderately unstable crack pattern. This would indicate that the bond was sufficiently stronger than the concrete, and the failure was a mixture of adhesive at the bond interface and cohesive in the substrate. The

bond was determined to be weaker and the light application methodology was not utilized. Additionally, the results from FRAC27_D were disregarded.

Table 2.3 SCCB Fracture Results for CFRP Specimens

Specimen	Critical Load, P_c	G_{Ic} (Initiation)	$f'c$
FRAC27_T	1743 N	515 J/m^2	40.85 MPa
FRAC27_D	1428 N	321 J/m^2	40.85 MPa
FRAC27_T1	1708 N	496 J/m^2	40.85 MPa
FRAC1031_T1	1223 N	254 J/m^2	36.89 MPa
FRAC1031_T2	1495 N	378 J/m^2	36.89 MPa
FRAC1031_T3	1223 N	254 J/m^2	36.89 MPa
FRAC27_T3	1068 N	279 J/m^2)	28.96 MPa
FRAC27_T4	1045 N	186 J/m^2	28.96 MPa
FRAC27_T5	1023 N	179 J/m^2	28.96 MPa

Referring to Figure 2.8, FRAC27_T experienced a strong/unstable crack pattern which would suggest that the failure was entirely cohesive in the concrete substrate, i.e. a brittle failure. Furthermore, the crack propagation extended in areas deep into the concrete substrate up to a quarter of an inch. This phenomenon is illustrated by Figure 2.9 with the circled area highlighting the deep substrate failure.

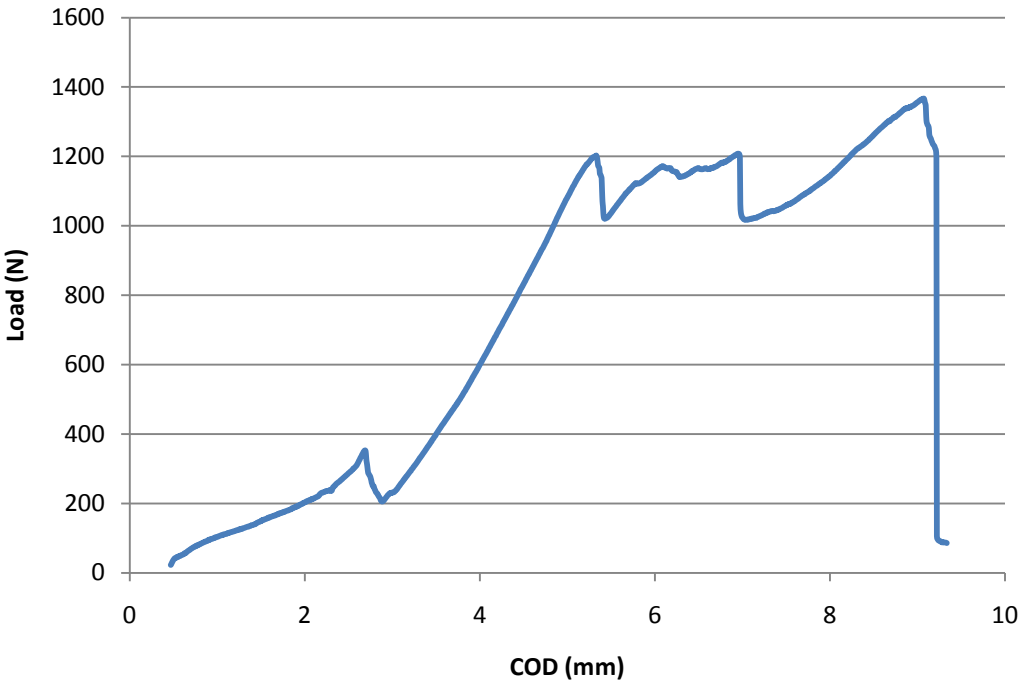

Figure 2.7 Fracture Energy – FRAC27_D

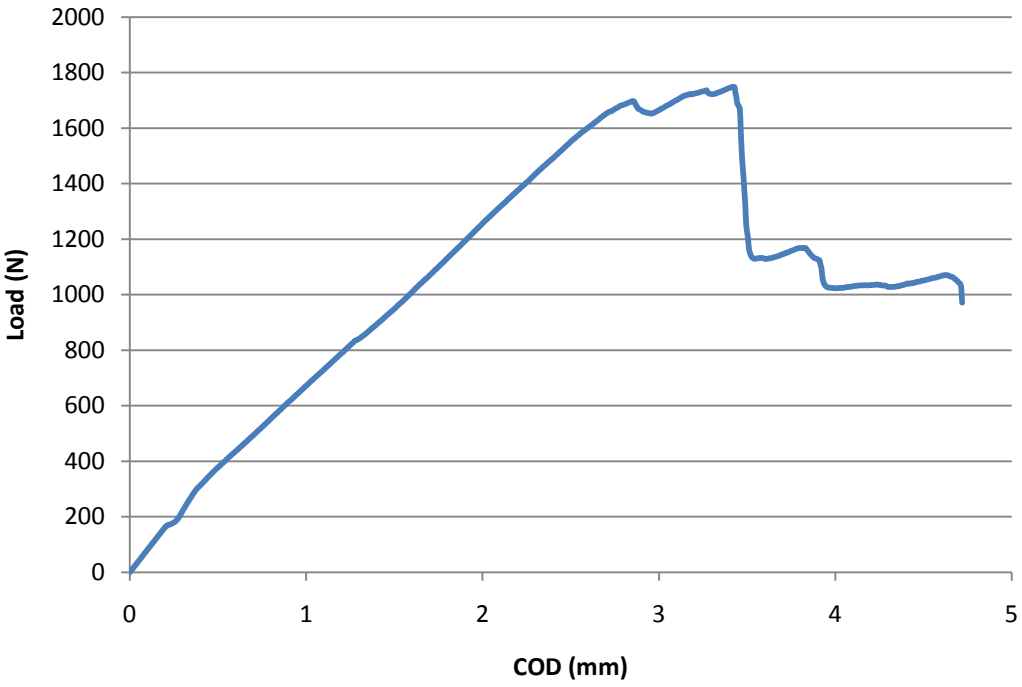

Figure 2.8 Fracture Energy – FRAC27_T

Figure 2.9 Deep Substrate Failure – FRACT27_T

The specimens FRAC27_T3, FRAC27_T4, FRAC27_T5 utilized a substrate with a compressive strength of 28.96 MPa at a graded concrete finish of SP 3. Due to the different crack growth patterns of the previously discussed specimens, a new application process was developed to provide a purely cohesive bond failure that could be categorized as strong/moderately unstable. The CFRP was impregnated per manufacturer's specifications but was applied with a FRP application roller (also permitted by Sika® application specifications). As can be seen by Figures 2.10 thru 2.12, the new application process achieved the desired crack propagation pattern. Even though each specimen exhibited a strong/moderately unstable crack pattern, the deep substrate failure was still evident and is presented in Figure 2.13. It should be noted that for the sake of brevity, all specimen results are not plotted herein but are included in all calculations.

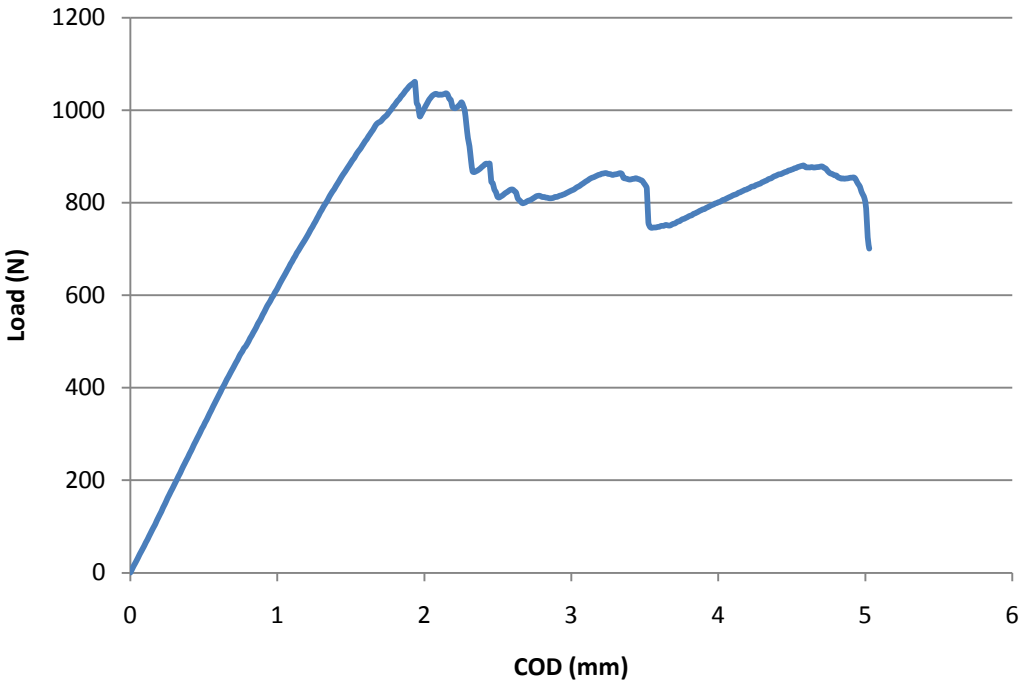

Figure 2.10 Fracture Energy – FRAC27_T3

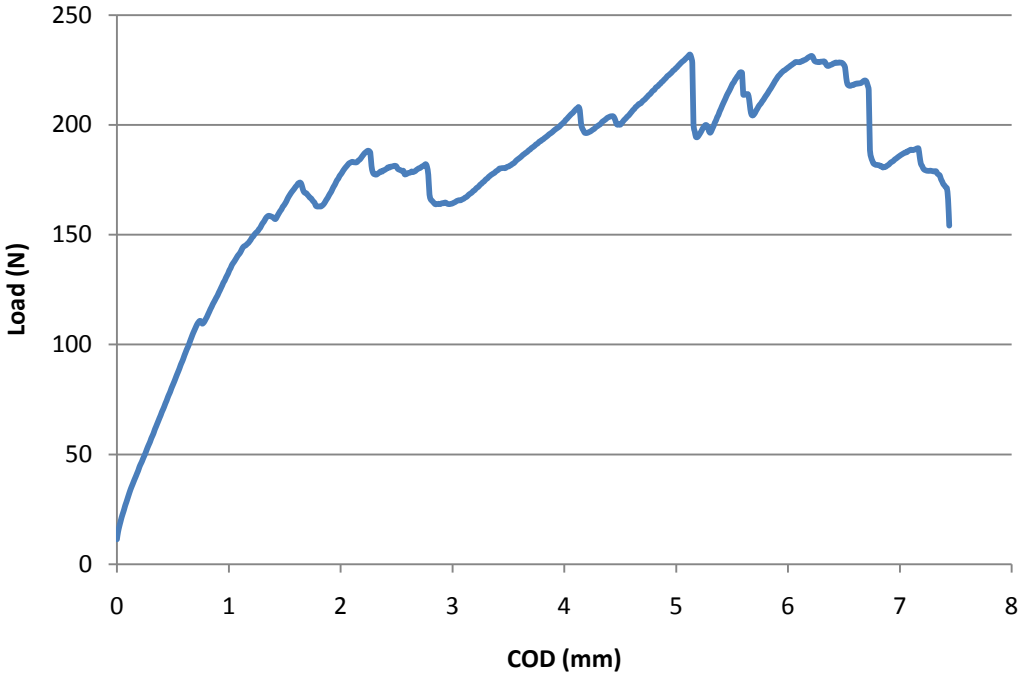

Figure 2.11 Fracture Energy – FRAC27_T4

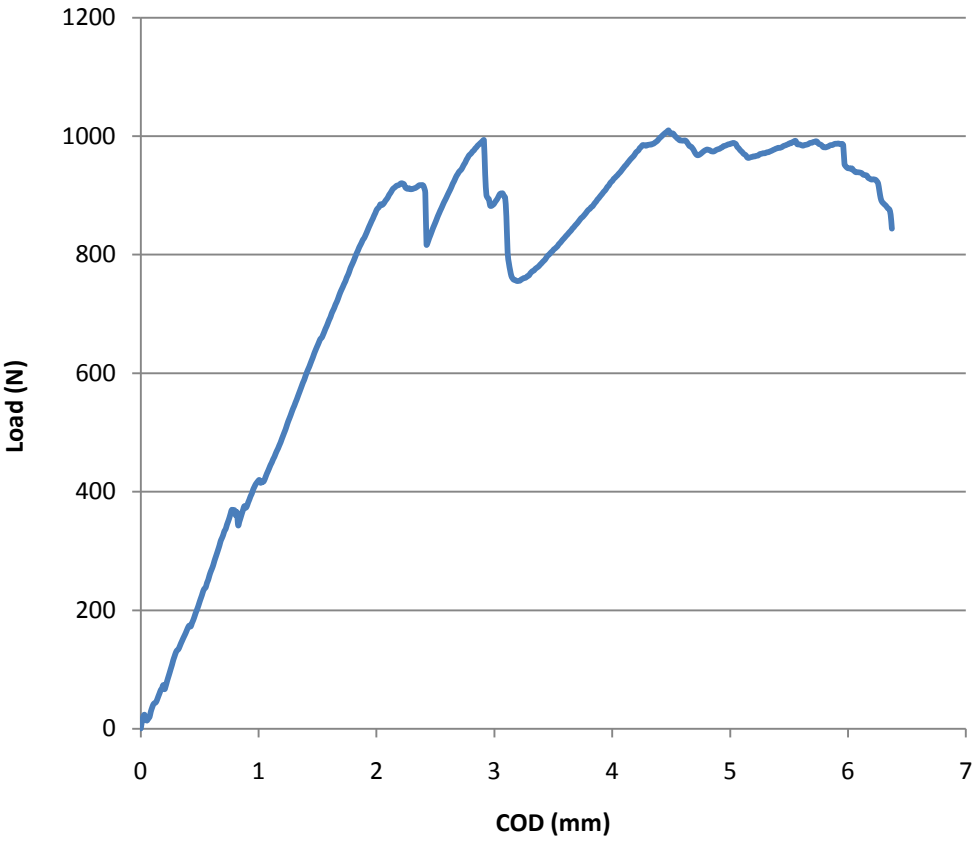

Figure 2.12 Fracture Energy – FRAC27_T5

Figure 2.13 Deep Substrate Failure – FRACT27_T4 and FRACT27_T5

Discussion

The two primary goals of the this work was to (1) define the behavior of the SP 3 surface profile as it pertains to Mode I fracture and to (2) determine the effects of the compressive strength of concrete on the strain energy release rate. As Boyajian (2002) developed the SCCB testing methodology utilized in this work and Lawrence and Boyajian (2006) investigated the impact of different surfaces in terms of the interface bond, it would be beneficial to compare the current results to those works. Referring to Figure 2.14, it is evident that the results of this study compares well with the surface

study performed by Lawrence and Boyajian (2006). The grey smeared area is a sum of the results from the current study compared to the multi-surface study which is represented by dark lines. Of particular interest is the bolded black line in Figure 2.14. This represents the surface utilized by Lawrence and Boyajian that approaches a SP 3 surface profile which falls inside the current study's boundary. It should be noted that the reason for the range of the bounded area (grey area) is that lower compressive strength concretes were used as well in this study, where Lawrence and Boyajian (2006) utilized the same concrete compressive strength with different surface preparations.

Caution, however, should be used in the straight comparison of the two studies due to the difference in the materials used for each study. The Lawrence and Boyajian (2006) study utilized an 59.98 MPa concrete mix with approximately a 1:1:1 mix ratio and a different CFRP system. Again referring to Figure 2.14, the maximum load for the Lawrence and Boyajian study was approximately 1557 N which was attained utilizing an 59.98 MPa substrate, while the current results produced a maximum of 1743 N with a 41.40 MPa substrate. Furthermore, Boyajian (2002) utilized an average substrate compressive stress of 51.57 MPa (approx. 1:3:5 mix ratio) that produced a critical load of approximately 1753 N.

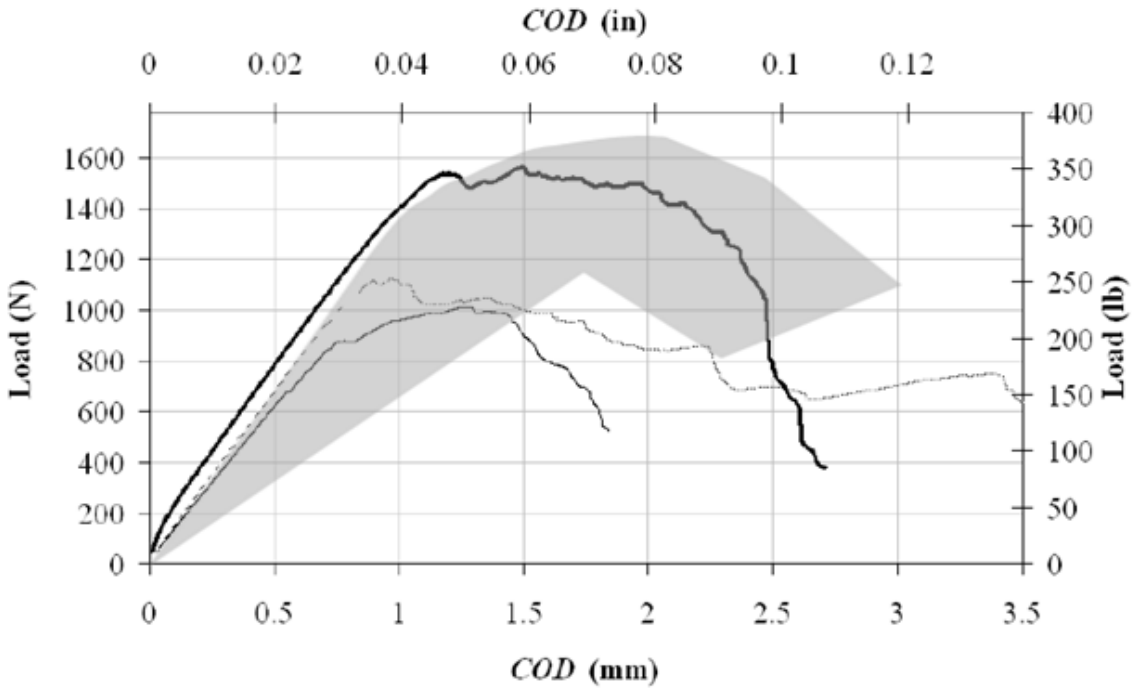

Figure 2.14 Comparison of Strain Energy Release Rate from Lawrence and Boyajian (dark lines) and Current Study (Smeared Grey Area).

Referring to Figure 2.15, it is evident that for the same mix ratio concrete, an increase in compressive strength correlates to an increase in the critical strain energy release rate when all data points are plotted with a confidence of $R^2 = 0.798$. Furthermore, when the critical strain energy release rate is averaged for each compressive strength, the confidence raises to $R^2 = 0.88$ as illustrated in Figure 2.16. In an effort to compare the multiple studies, the following linear relationship will be used to normalize the data presented by the previous studies:

$$G_{Ic} = 23.719 f_c' - 520.59 \qquad (2\text{-}2)$$

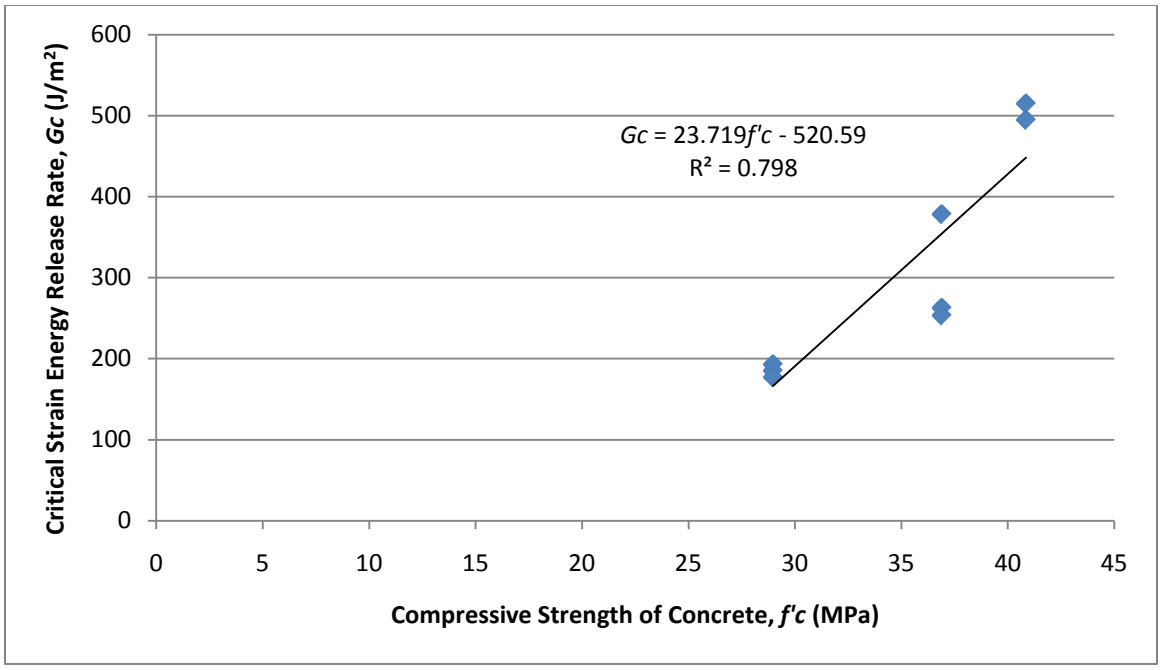

Figure 2.15 Critical Strain Energy Release Rate as a Function of Concrete Compressive Strength.

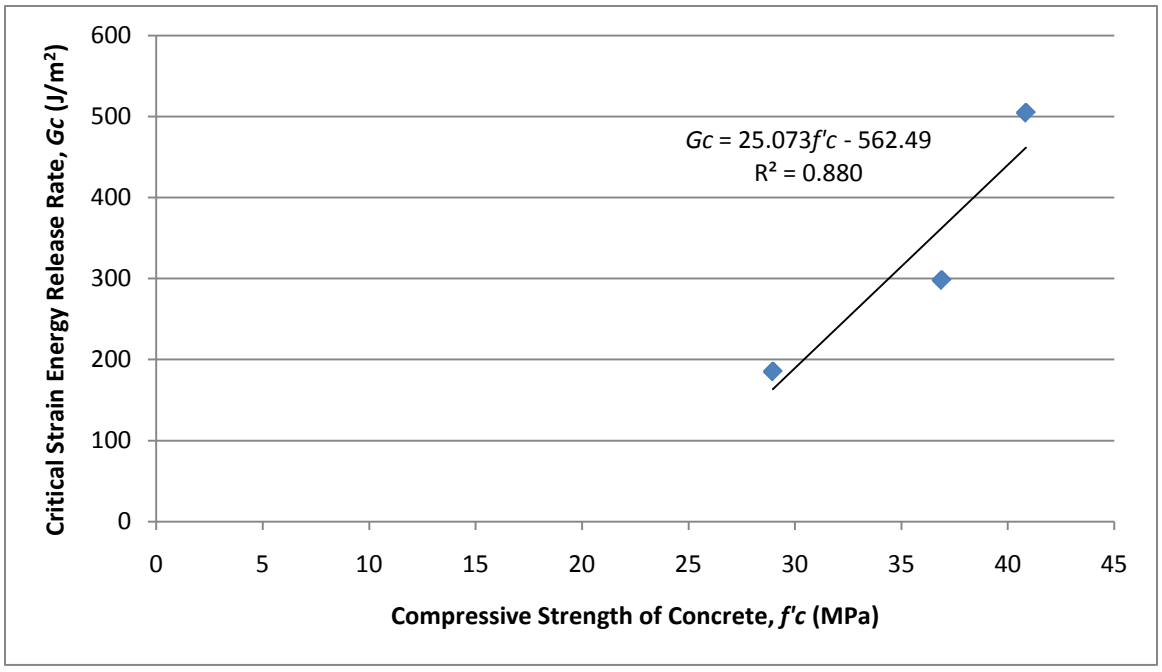

Figure 2.16 Average Critical Strain Energy Release Rate as a Function of Concrete Compressive Strength.

Utilizing the compressive strength of concrete from Boyajian (2002), Equations 2-1 and 2-2 yield a critical strain energy release rate of 646 J/m^2 and a critical load of 1886 N. The average reported critical load from the work was 1739 N which produced a critical strain energy release rate of 552 J/m^2. This produced a difference of 142 N (8 %) in critical load and 95 J/m^2 (15%) in critical strain energy release rate well within the current study's sample range. It should be noted as well, that the Boyajian (2002) study utilized a different CFRP system than the current study which could account for the minor differences. Referring to Figure 2.17, when Boyajian's work (red highlight) is plotted with the current study's data the confidence increases to a $R^2 = 0.80$.

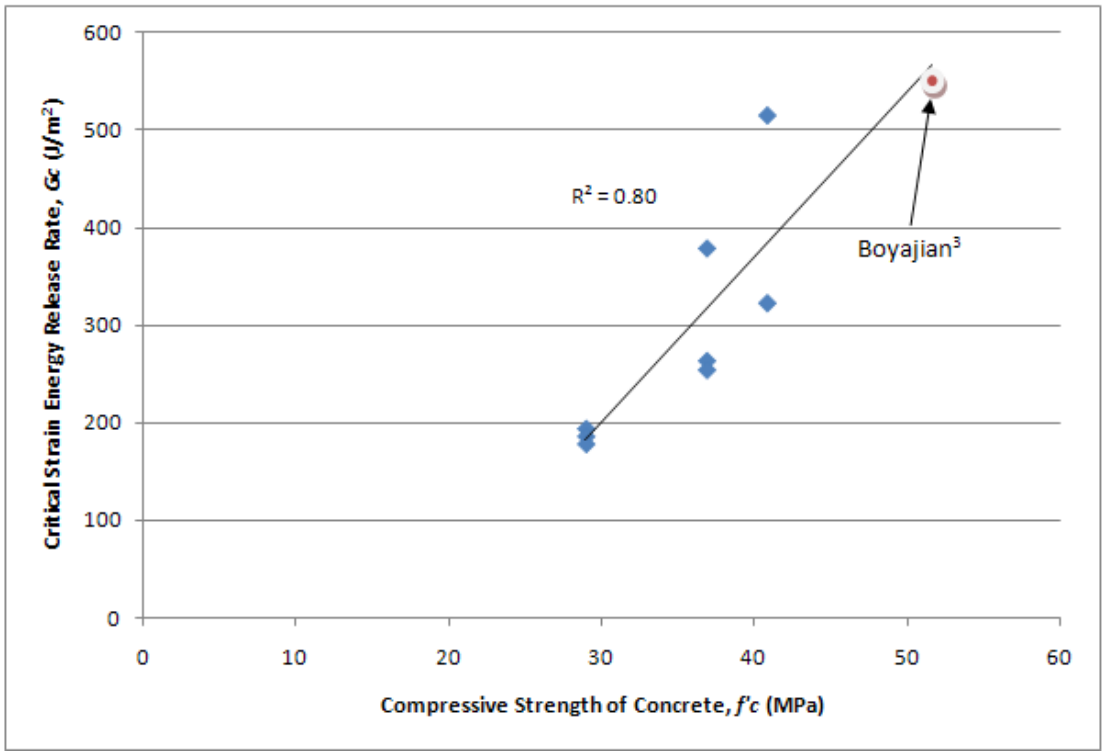

Figure 2.17 Average Critical Strain Energy Release Rate as a Function of Concrete Compressive Strength with Boyajian (2002) Averaged Data Included.

Performing the same calculation for the Lawrence and Boyajian (2006) study, Equations 2-1 and 2-2 provide a critical strain energy release rate of 937 J/m^2 and a critical load of 2709 N. However, that study produced an actual strain energy release rate, for the sand blasted specimens, of 309 J/m^2 (67 %) and a critical load of 1546 N (43%). Clearly, these results do not correlate with the findings of the current study. At this point, it is important to revisit the mix designs and surfaces utilized in the studies. Boyajian (2002) and the current study utilized approximately 1:3:5 mix ratios with treated surfaces (although, Boyajian's surfaces were not quite treated to SP 3 surface roughness), while Lawrence and Boyajian (2006) utilized approximately a 1:1:1 mix ratio and a sand-blasted surface. The 1:1:1 mix ratio produced a surface that exposed equal amounts of aggregate and paste, of which, the paste would provide less strength. It should be intuitive to infer that the rougher surface provides a better binding surface, however, the results of the current analysis clearly indicate that the mix ratio in conjunction with the compressive strength of concrete influences the critical strain energy release rate of the system. It should also be noted, that this current study is not claiming that the Lawrence and Boyajian study is incorrect, merely, that each concrete mix ratio produces different results.

Conclusions

In the closing of the work by Boyajian et al. (2005), the authors raised the question that critical strain energy release rate may be impacted by mix design, aggregate size, manufacture of the SCCB, etc. and only when these variables are constant can the critical strain energy be constant. In an effort to address these issues, this work provided the following:

1. The work illustrated that given a consistent surface preparation and mix ratio, the critical strain energy release rate increases as the compressive strength of concrete increases.
2. The SP 3 surface profile provided a strong enough bond that resulted in deep penetrations into the concrete substrate.

Future Directions

The results of this study show that the surface profile aids in producing a bond strength that far exceeds the strength of the concrete substrate and therefore the critical strain energy release rate is primarily a function of the compressive strength of the concrete and the mix ratio used. This is evidenced by the cohesive failures discovered, post fracture; therefore, the fracture energies in this study may primarily be characterized as being a function of the tensile resistance of the concrete itself. However, a review of studies performed by Moavenzadeh and Kuguel (1969); Kaplan (1961); Brown (1972); and Jenq and Shah (1985) showed that the fracture energy of concrete from the current study is significantly higher than their reported values. The only conclusion can be that even with the deep penetration into the concrete substrate, there exists a contribution from the CFRP system or geometry of the contour. This deep substrate failure was not readily experienced in previous SCCB studies and therefore determining its cause should become a focus of future analytical studies at the microscopic level.

While this study confirms that the bond strength of pristine concrete to CFRP specimens is a function of substrate compressive strength, only normal concrete, i.e. $f'_c <$ 41.4 MPa has been tested. Further testing would be required for bond behavior of high strength concretes. Furthermore, fracture studies of the ICRI surface profile should be

performed for specimens that have been subjected to freeze-thaw cycles and wet-dry cycles for both normal concrete and high performance concrete.

CHAPTER 3: FINITE ELEMENT ANALYSIS OF THE SINGLE CONTOURED CANTILIVER BEAM

Submitted to the International *Journal of Composites Part B*

Finite Element Modeling of the Mode 1 Failure of the Single Contoured Cantilever CFRP-Reinforced Concrete Beams

T. Nicholas[a], D. Boyajian[b], S.E. Chen[c] and A. Zhou[d]

Abstract

The Single Contour Cantilever Beam (SCCB) test method has been developed with the intent to capture Mode I opening failures of CFRP-reinforced concrete beams. Recent development in the method explores possible shifting damage into the concrete substrate by using the ICRI surface profile level three (SP3) as the desired CFRP bonded interface to concrete. To validate and explain the interface fracture behavior, finite element analysis using special cohesive elements has been performed. The cohesive element allows separation of the concrete substrate from the CFRP. This paper presents the simulation of laboratory test results where failure in the substrates has been successfully reproduced. The simulation results indicate that finite element method using cohesive elements can successfully replicate the Mode I critical strain energy release rate and the peak capacity of the laboratory tests, and may have the potential to simulate actual applications.

KEYWORDS: concrete repair; Mode 1 fracture; cohesive elements, finite element model

[a] Thomas Nicholas, University of North Carolina at Charlotte, Charlotte NC 28223
[b] David M. Boyajian, Taylor University, Upland, IN 46989
[c] Shen-en Chen, University of North Carolina at Charlotte, Charlotte NC 28223
[d] Aixi Zhou, University of North Carolina at Charlotte, Charlotte NC 28223

Introduction

Several laboratory methodologies have been developed over the past few years to measure the Mode I critical strain energy release rate involving composite wrapped concrete beams. Failures of Representative methodologies designed to isolate Mode I opening failure of a fracture interface include the modified double cantilever beam (DCB) method (Guirgiutiu et al, 2001), the peel test method (Karbhari and Engineer, 1996), the membrane peeling method (Kimpara, et al. 1999), and the single contour cantilever beam (SCCB) (Boyajina, et al., 2002). All the above methods are variations of each other with different strengths and weaknesses, depending on the application. However, the SCCB method exclusively ensures that the failure will always be the first mode. A second advantage of the SCCB method is the elimination of compliance measurements.

The SCCB method was first developed by Boyajian (2002) and has been utilized to determine the critical strain energy release rates at the bonding interface between concrete and carbon fiber reinforced polymer (CFRP) (Boyajina, et al., 2002); (Kodkani, 2004); and Lawrence and Boyajian (2006). Figure 3.1 shows the schematics of the SCCB test including the test specimen that consists of concrete base plate, FRP bonded layer, the wood contour, and the experimental setup that includes a steel strap for pulling on the wood contour. Figure 3.2(a) shows the actual test setup within a MTS® test apparatus with arrow indicating direction of pull load. With the SCCB test, the high tensile capacity LVL is loaded with a normal force, **P**, inducing Mode I failure behavior of the FRP to concrete interface and thus avoiding the arm break-off failure.

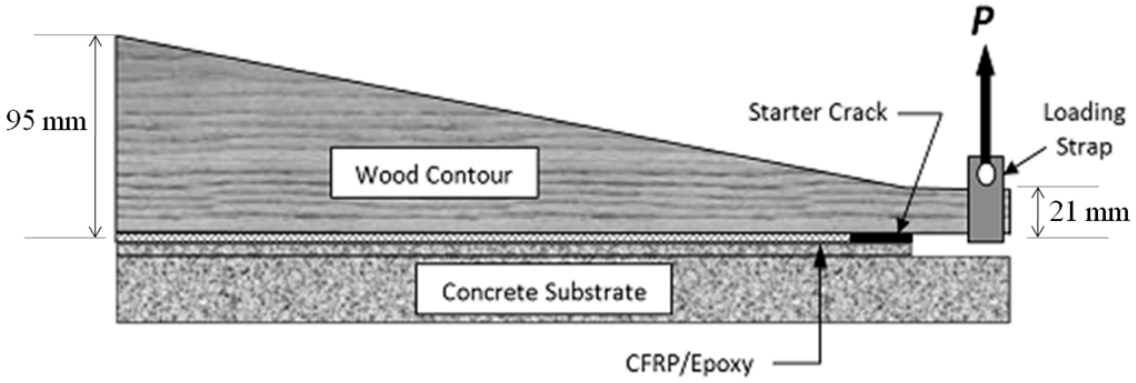

Figure 3.1 Schematic of Single Contoured Cantilever Beam Test

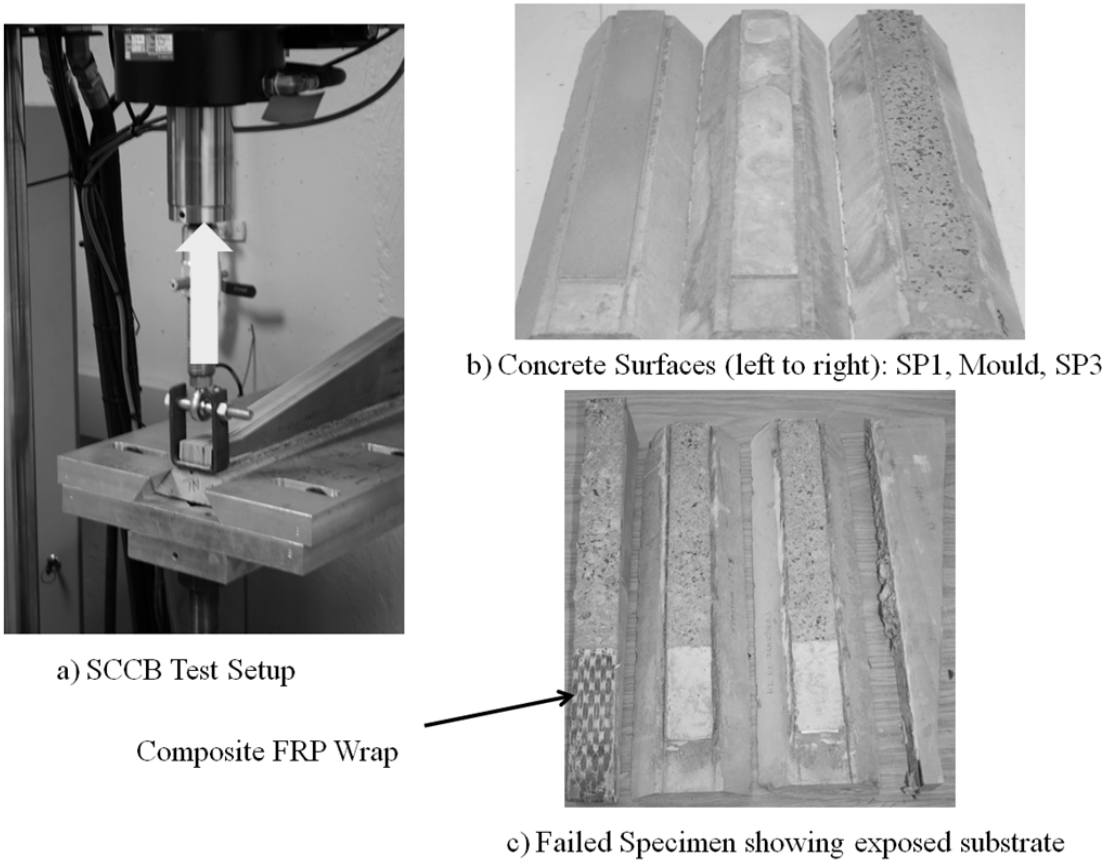

Figure 3.2 The SCCB Test: a) Experimental Setup (Arrow Indicating Load Direction); b) Different Concrete Surfaces (SP1, Mould, SP3); c) Interface Face of Failed Specimens

The current study focused on using the International Concrete Repair Institute surface preparation 3 (ICRI SP3) (ICRI, 2003) method to ensure failure within the substrate. Figure 3.2(b) shows the different surface areas: SP1, mould and SP3. Study of failure in the substrates is important since it may lead to premature failure and brittle failures (Buyukozturk, et al., 2004). Figure 3.2(c) shows the failed specimens clearly indicating failure within concrete substrate.

This paper reports Finite Element (FE) simulation of a series of SCCB tests conducted with concrete specimens prepared with SP3 surfaces, which was not previously attempted. In order to develop realistic FE models, a damage evolution approach has been adopted. The results presented shows that the approach effectively predicts the critical strain energy release rate of the bonded interface. The model also compares well with the laboratory test results.

Mode 1 Fracture

Fracture behavior can normally be characterized as beginning with crack-initiation and intensifying through crack propagation. At the onset of crack initiation, the crack propagation behavior becomes a function of the displacement of the failed interface surfaces (Berry, 1963 and Boresi, 1993). Irwin (1958) defined three failure modes to describe how the surfaces are displaced by Mode I, Mode II and Mode III failures. Mode I describes a failure of the interface bond that occurs normal to the failed surface, often referred to as the opening mode. While most fractures can be described by one of the failure modes, the mixing of mode failures, such as, Mode I – Mode II is also a possibility. The ability of an engineering material to resist these failure modes is frequently referred to as fracture toughness. The commonly accepted method for

representing fracture toughness is the critical release strain energy, G_C, as defined by the Irwin-Kies equation (Irwin and Kies, 1954):

$$G_C = \left(\frac{P_C^{\,2}}{2b}\right)\left(\frac{dC}{da}\right) \tag{3-1}$$

Where:

G_C = Critical strain energy release rate (J/m^2)

P_C = Critical load (N)

b = width of the specimen (mm)

dC/da = Rate of compliance (C) with respect to crack length (a) (N^{-1})

Analytical Modeling of Fracture and the Cohesive Elements

As it pertains to the current study, finite element modeling of the SCCB can be divided into two categories: compliance of the SCCB wood contour and fracture. As there exists a number of methods to model crack propagation, it is important to select an efficient and accurate representation of the failure behavior. While the SCCB has not specifically been modeled for fracture, a number of past studies have focused on fracture of the double cantilever beam and the peel test. Most recently, Turon et al. (2007), Huang and Lyons (2005), and Diehl (2008) proposed methodologies for modeling the DCB, a modified DCB and a peel test, respectively. For each study, the model was used to determine the total energy required to propagate the crack tip. The total energy required to fracture concrete can be taken as:

$$G_f = \frac{1}{B*(W-a)} \int P \, d\delta \tag{3-2}$$

where

G_f = Specific fracture energy (J/m^2)
B = specimen thickness (mm)
W = fracture width (mm)
a = initial crack length (mm)
P = point load (N)
δ = displacement perpendicular to crack length (mm)

Huang and Lyons (2005) employed the J-integral algorithm in ABAQUS® to model the crack propagation of a modified DCB as well as to calculate the critical strain energy release rate. The methodology produced good results compared to the basic energy equation and laboratory results. However, according to Turon et al. (2007), the cohesive element is an efficient approach to modeling fracture, as well, when the crack propagation is known *a priori*.

Diehl (2008) proposed utilizing an ABAQUS® cohesive element to model the bonded region between elastic and inelastic materials, namely a thin film. In the study, a penalty based approach to debonding was proposed. In the penalty approach or damage evolution, as the elements ultimate stress capacity (traction, t_{ULT}) is achieved, the element is deleted from the model and does not provide further resistance to load. This damage process is illustrated by Figure 3.3, where the ultimate nominal stress serves as the elastic limit and the area under the curve provides the critical fracture energy, G_c. While Diehl did not compare the results to laboratory testing, this "unzipping" behavior closely resembles the behavior of the SCCB during crack propagation. Therefore, the cohesive element was used to model the bond interface in current study.

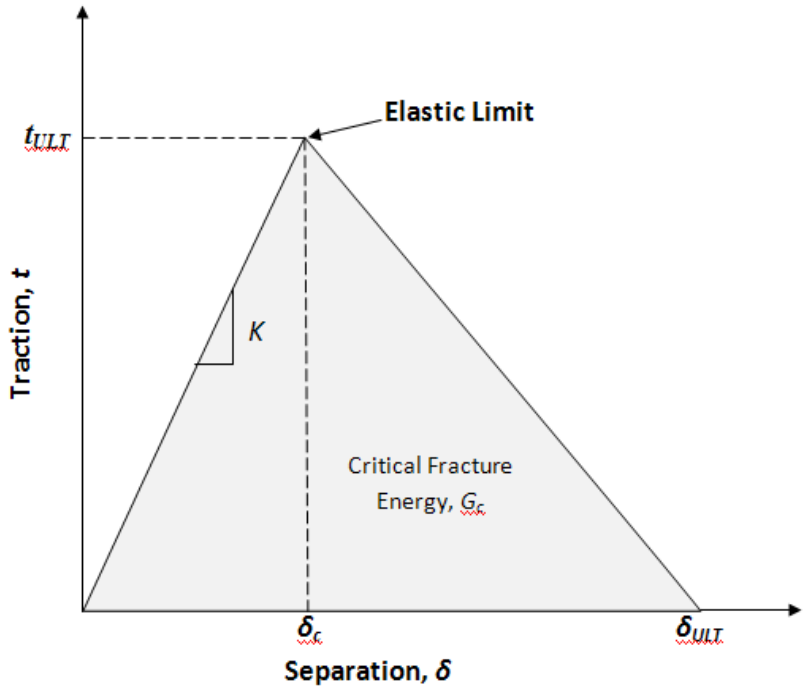

Figure 3.3 Damage Evolution Curve for ABAQUS Cohesive Element

ABAQUS® assumes that traction separation is linear elastic prior to undergoing complete damage evolution. The elastic behavior is represented by a constitutive matrix in terms of nominal stress and strain. While ABAQUS® provides a three dimensional model, torsional effects will not be presented here due to only a two dimensional model was employed. It should be noted, that while a mixed mode process may be present (normal and shear), the SCCB test inherently provides a Mode I failure which is predominantly normal to the interface. Given that the nominal stress can be written as (ABAQUS®, 2007):

$$\boldsymbol{t_{ULT}} = \{\boldsymbol{t_n^0}\} \tag{3-3}$$

where $\boldsymbol{t}$ = total separation stress

$\boldsymbol{t_n}$ = normal separation stress

and strain can be written as

$$\boldsymbol{\varepsilon} = \{\boldsymbol{\varepsilon_n}\} \tag{3-4}$$

where $\boldsymbol{\varepsilon}$ = total separation strain

$\boldsymbol{\varepsilon_n} = \frac{\boldsymbol{\delta_n}}{\boldsymbol{T_o}}$, normal separation strain.

The elastic behavior can then be written as follows:

$$\boldsymbol{t_{ULT}} = \{\boldsymbol{t_n^0}\} = [K_n]\{\boldsymbol{\varepsilon_n}\} = K\varepsilon \tag{3-5}$$

where K = the stiffness that relates to the nominal stress. The subscripts for the stiffness matrix represents again normal separation (n).

Following the initial elastic response, damage is initiated provided that one of the user defined criterion are met. The damage initiation criteria can be defined in ABAQUS® utilizing stress, strain or quadratic function. The current work utilized a maximum stress criterion as follows (ABAQUS®, 2007):

$$\max\left\{\frac{\langle t_n \rangle}{t_n^0}\right\} = 1 \tag{3-6}$$

where $\langle t_n \rangle$ = normal stress state

t_n^0 = peak normal stress

Once the damage criterion is achieved, the material undergoes a softening process or loss of stiffness that perpetuates the damage evolution. ABAQUS® (ABAQUS®, 2007) represents damage evolution by introducing the damage variable, D, which ranges in magnitude from 0 to 1. The effect of the damage variable is given by

$$t_n^0 = \begin{cases} (1-D)t_{nd} \\ t_{nd} \end{cases} \tag{3-7}$$

where t_{nd} = predicted normal stress (undamaged)

D = damage variable

Laboratory SCCB Tests

A series of SCCB tests was carried out and was presented in Chapter 2 of this work. The single cantilever contoured beam (SCCB) used for this study is comprised of a substrate material (reinforced concrete), a fiber reinforced polymer layer and a wood contour as illustrated in Figure 3.1. This study utilized the previously calibrated contour developed by Lawrence and Boyajian (2006) with a rise of 95 mm. In this study, normal weight concrete with a target compressive strength of 41.4 MPa was used. The contour material used in the study is a wood product: 1.9E Microllam® LVL (Laminated Veneer Lumber, Weyerhaeuser). Additionally, the FRP system selected for the study was Sikadur® 301 two-part epoxy and SikaWrap® Hex 103C carbon fiber.

The pull test results are presented in Table 3.1 where G_C and P_C for three different tests are presented along with the averaged values. Figure 3.2(c) shows the typical failed specimens where failure plane showed exposed aggregates embedded in the substrates. Failure plane for all tests falls within the concrete matrix and lies within the substrate. Figure 3.4 shows the critical load vs. crack opening displacement from the test results.

Table 3.1 Experimental and Analytical Results

Specimen	Critical Load, P_c	G_{Ic} (Initiation)	$f'c$
FRAC1031_T1	1494 N	384 J/m^2	37 MPa
FRAC1031_T2	1245 N	267 J/m^2	37 MPa
FRAC27_T3	1045 N	183 J/m^2	29 MPa
Average	1261 N	278 J/m^2	34 MPa
Finite Element	1352 N	307 J/m^2	37 MPa

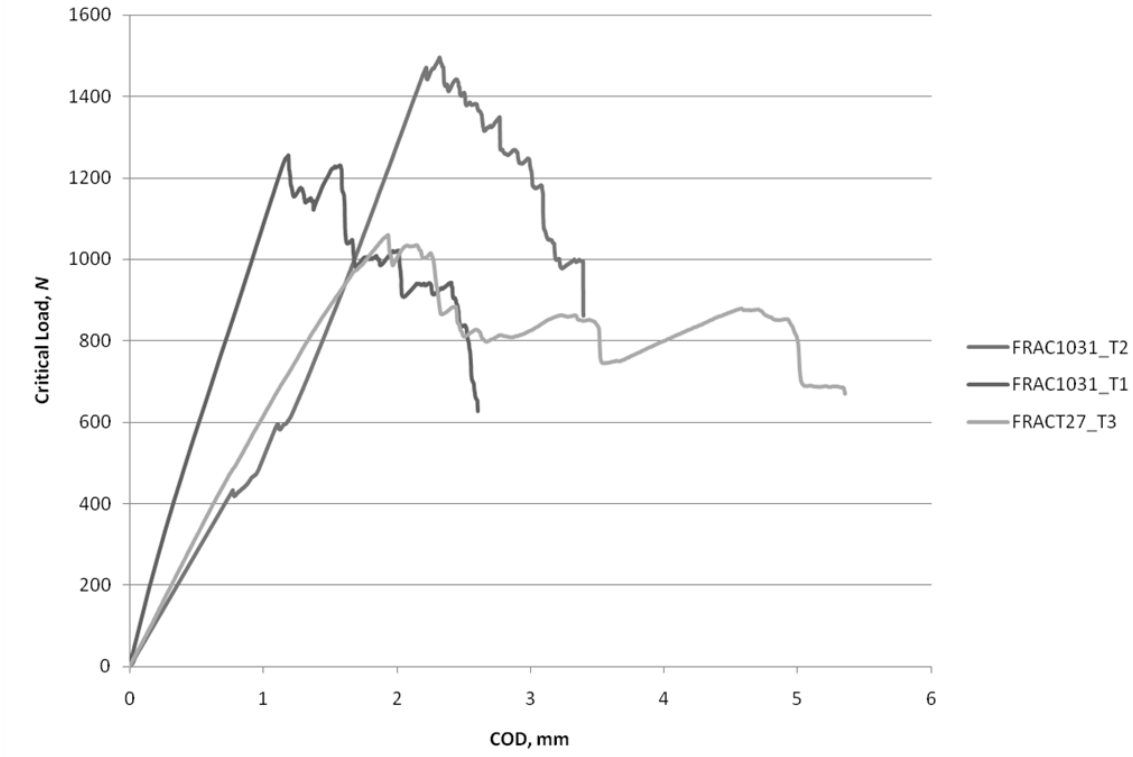

Figure 3.4 Critical Strain Energy Curves

SCCB Analytical Model

The SCCB was modeled using 2D plain strain plate quad elements in ABAQUS® and represents the LVL contour, the concrete substrate, and the CFRP layer. For FRP laminates, typically orthotrpic layer elements are used (Giurgiutiu, et al., 2004), however, for the 2D model, non-directional element is used.

The interface region was geometrically inputted to represent a mixed layer of concrete and epoxy due to the deep intrusion of crack propagation into the substrate. This interfacial zone was considered to be the cohesive layer and was modeled using ABAQUS® cohesive element, COH2D4. The material properties required to model the cohesive element are G_c, K, nominal stress (traction), t, and separation, δ. The system was subjected to a 1.78 mm deflection of the contour tip, which corresponds to the laboratory results for the crack opening displacement (*COD*) at the critical load, P_c.

Figure 3.5 shows the FE model. Due to the deviation in concrete properties, averaged material properties are used for the cohesive element: G_c = 133.97 J/m^2; K = 102.45 N/m^3 and nominal stress, 15.51 MPa. Table 3.2 provides a material summary for the SCCB model. The one area of concern in utilizing the cohesive element, as Duan et al. (2007) pointed out is the element size. Duan et al. (2007) and others have proposed various analytical processes for determining cohesive element size and Diehl (2008) proposed an element size of one fifth of the model. The size of the cohesive element was 1/10 the size of the CFRP layer with an aspect ratio of 1 to 5. A close-up view of the final model is shown in Figure 3.6.

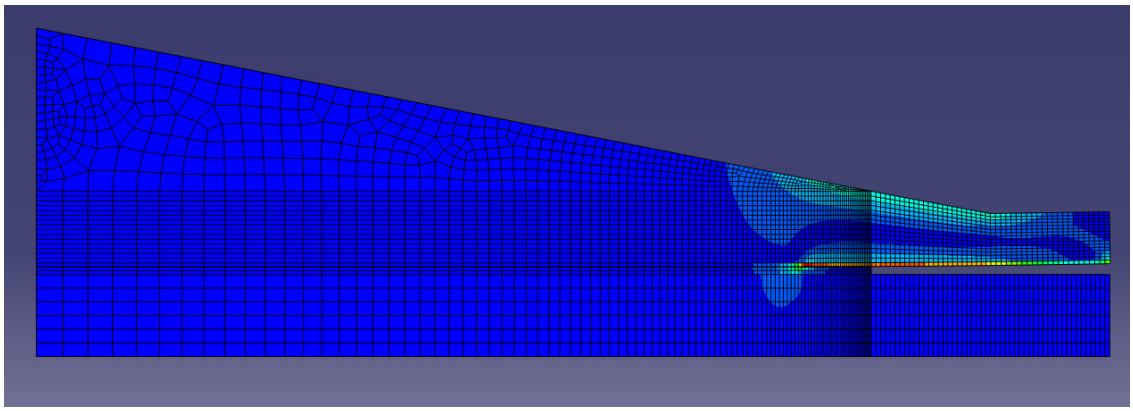

Figure 3.5 Finite Element Model of the SCCB Utilizing Cohesive Element

Table 3.2 Summary of FE Material Input Values

Material	Young's Modulus	Poisson's Ratio	Fracture Energy
Concrete	30 GPa	0.18	N/A
LVL Contour	13 GPa	0.30	N/A
Cohesive	102 GPa	N/A	134 J/m^2
CFRP	235 GPa	0.15	N/A

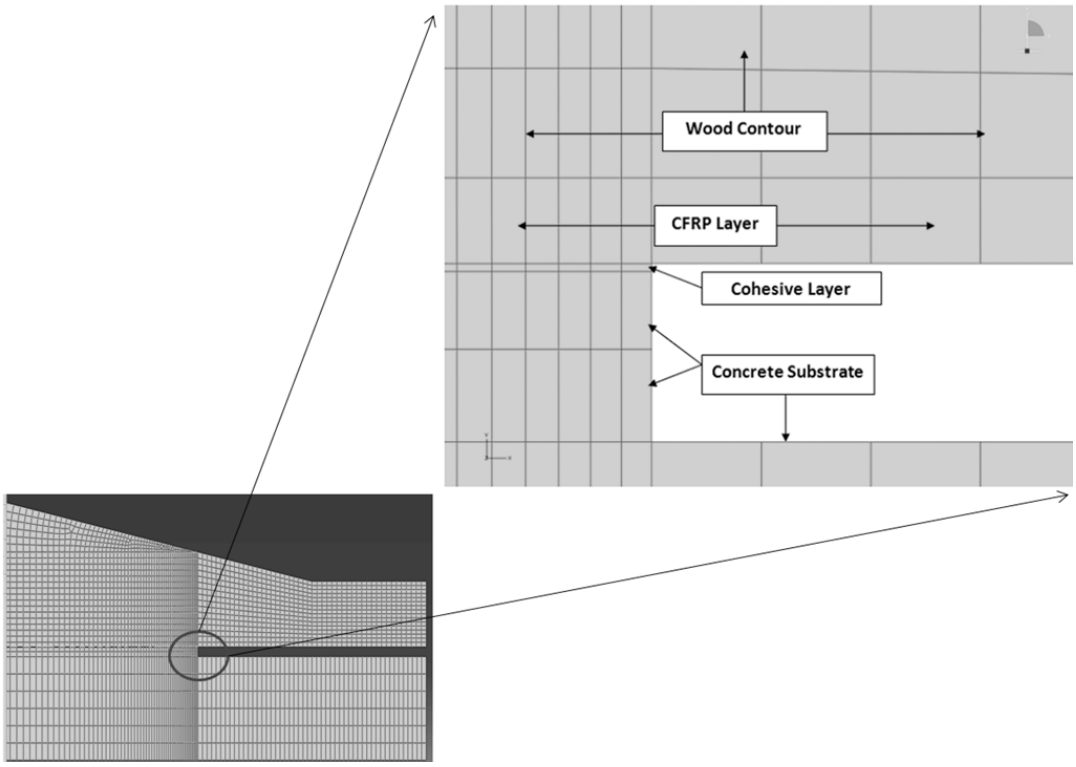

Figure 3.6 The Finite Element SCCB Model

Results and Discussion

Figure 3.7 shows the stress distribution at critical load, significant crack propagation has penetrated into the interface. Over 50 cohesive elements have been removed (delamination) immediately after the critical load was achieved. Also illustrated in Figure 3.5, the stress distribution in the wood layer displayed typical Bernoulli bending behavior with compressive stresses of the cantilever at the top and the tensile stresses at the bottom. However, during the first fracture sequence of the SCCB, the interface was represented by a region of discontinuity as it pertains to the stress. The discontinuity is a result of the different material properties between the cohesive element, the concrete and the FRP. The maximum stress in the FRP material is 48.46 MPa, which occurs at the crack tip, indicating the composite wrap is being stressed.

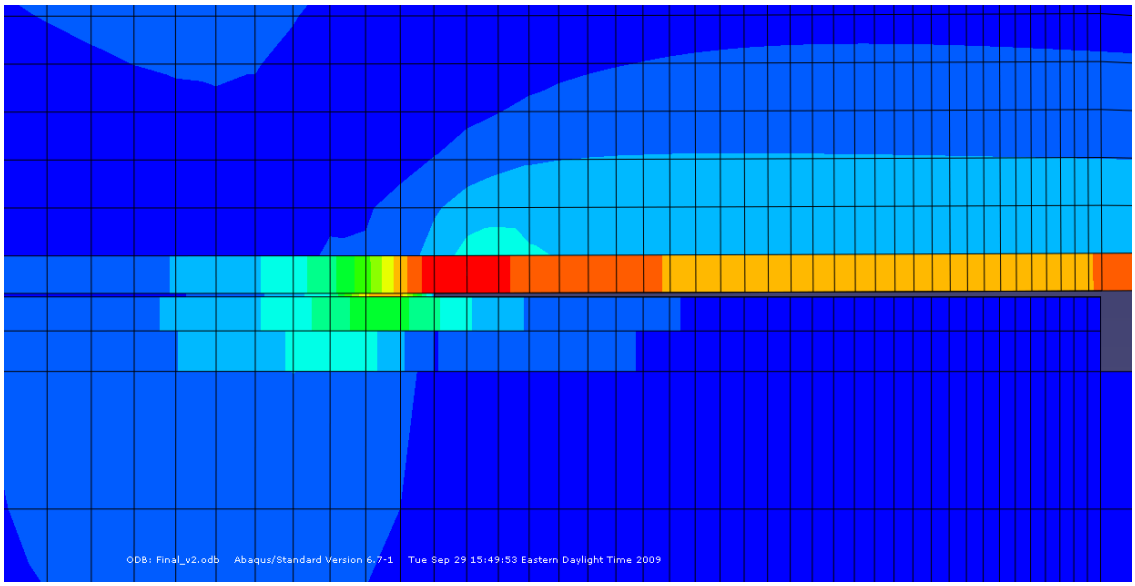

Figure 3.7 Close-Up Rendering of the Damage Evolution of the Cohesive Element

Figure 3.8 shows the stiffness degradation within the interface (cohesive elements) and behind the crack. The analytical model produced reasonably close results compared to the laboratory results (Figure 3.9). Figure 3.9 is a rendering of the numerical model results as a function of all fractured specimens represented by the smeared gray area, indicating the experimental deviations. It should be noted that the laboratory results actually represent various compressive strengths of concrete, ranging from 29.0 MPa to 41.4 MPa. This will somewhat affect the specific fracture energy of the concrete as well as the effective stiffness of the cohesive layer.

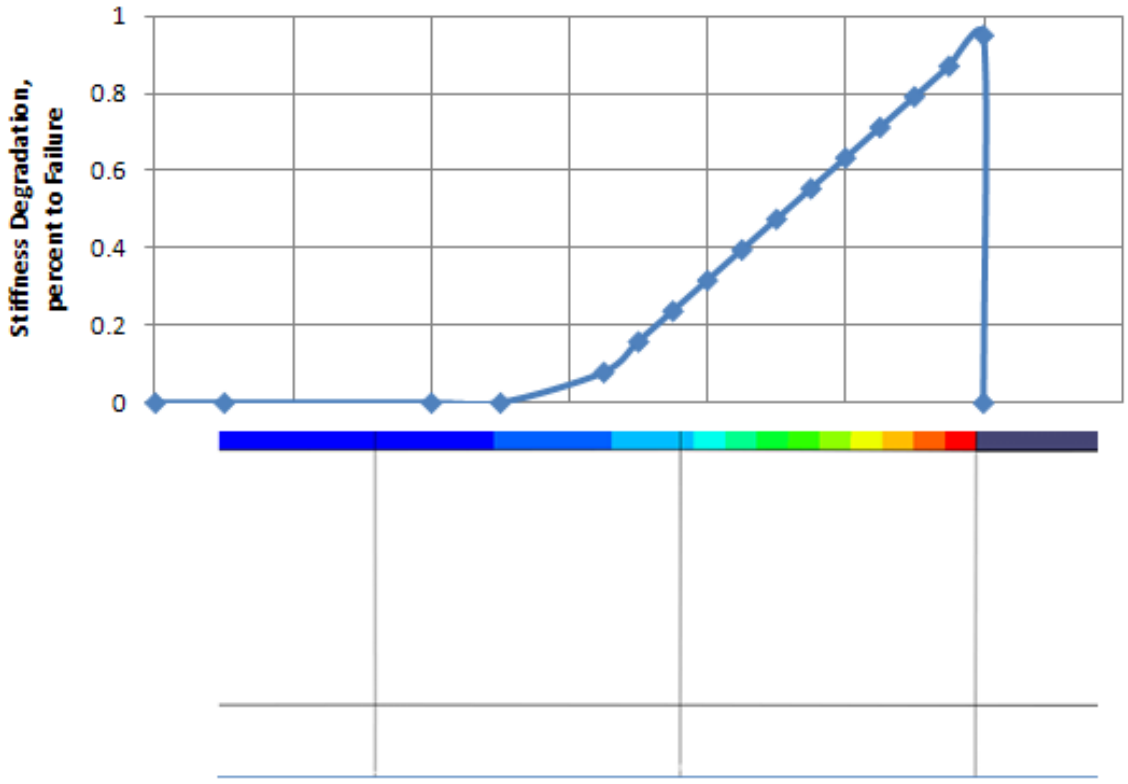

Figure 3.8 Stiffness Degradation along the Cohesive Zone (Crack Propagation) Including the Stiffness Degradation Behind the Crack

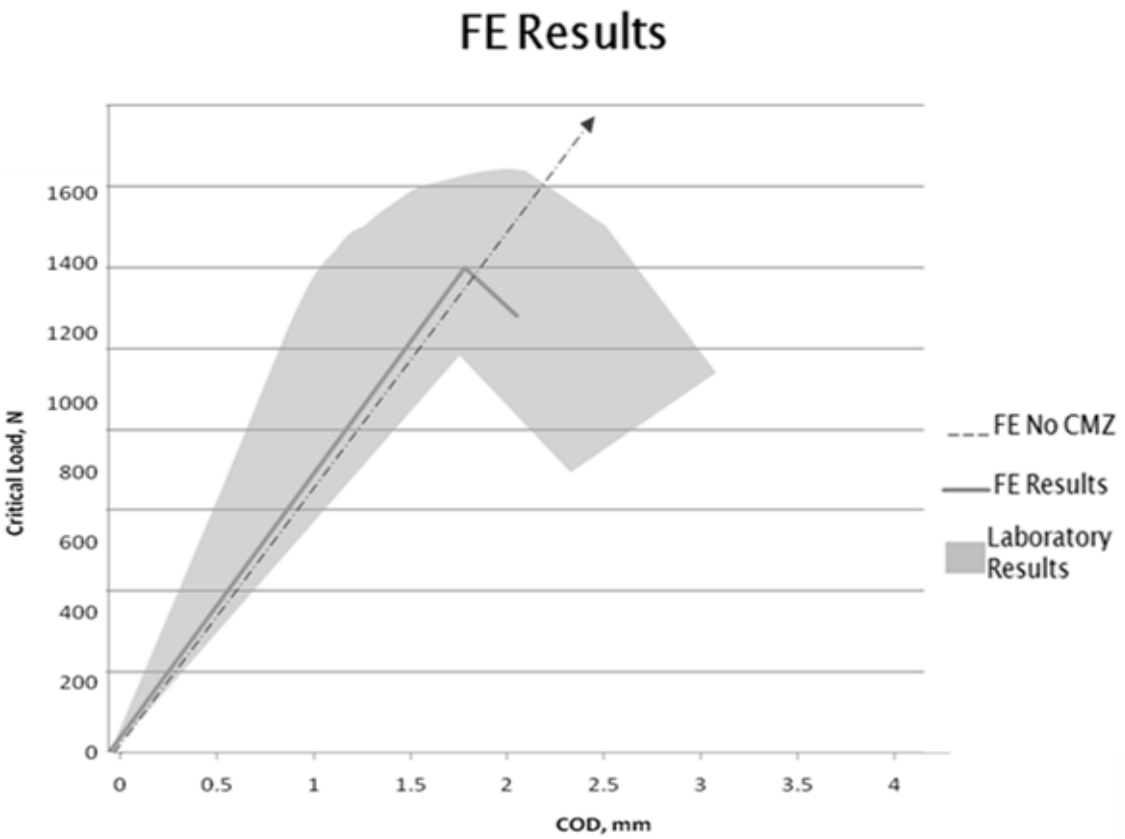

Figure 3.9 Finite Element Results Compared to the Companion Laboratory Results (Straight Line Indicating Non-Separation Model with no CMZ)

The critical load, Pc, was determined to be 1352 N at a crack opening displacement of 1.78 mm. The averaged critical load from the laboratory results was 1361 N at a crack opening displacement of 1.70 mm yielding a percent difference of approximately 2 percent and 4 percent, respectively. The critical strain energy release rate from the finite element analysis was then calculated as 307 J/m^2, which also corresponded well with the averaged critical strain energy release rate of 278 J/m^2. While the numerical results are acceptable, the behavior of the modeled fracture varied somewhat from the laboratory results. The fracture produced in the model is more representative of stable crack propagation rather than the moderately unstable fracture pattern produced in the laboratory experiments.

Result from FE model with no cohesive material zone (CMZ) is also investigated, which shows significantly larger critical ultimate stress (straight line in Figure 3.8). Figure 3.10 shows the stress concentration in the non-separation model, where the peak stress is at initial fracture point is 71.6 MPa. Since the model is not allowed to crack, the FRP composite does not demonstrate realistic stress distribution as indicated in Figure 3.6.

It is also of interest to note that high stress concentration exists within the concrete elements during loading (Figure 3.5), accurately portrayed possible penetrating into the substrate.

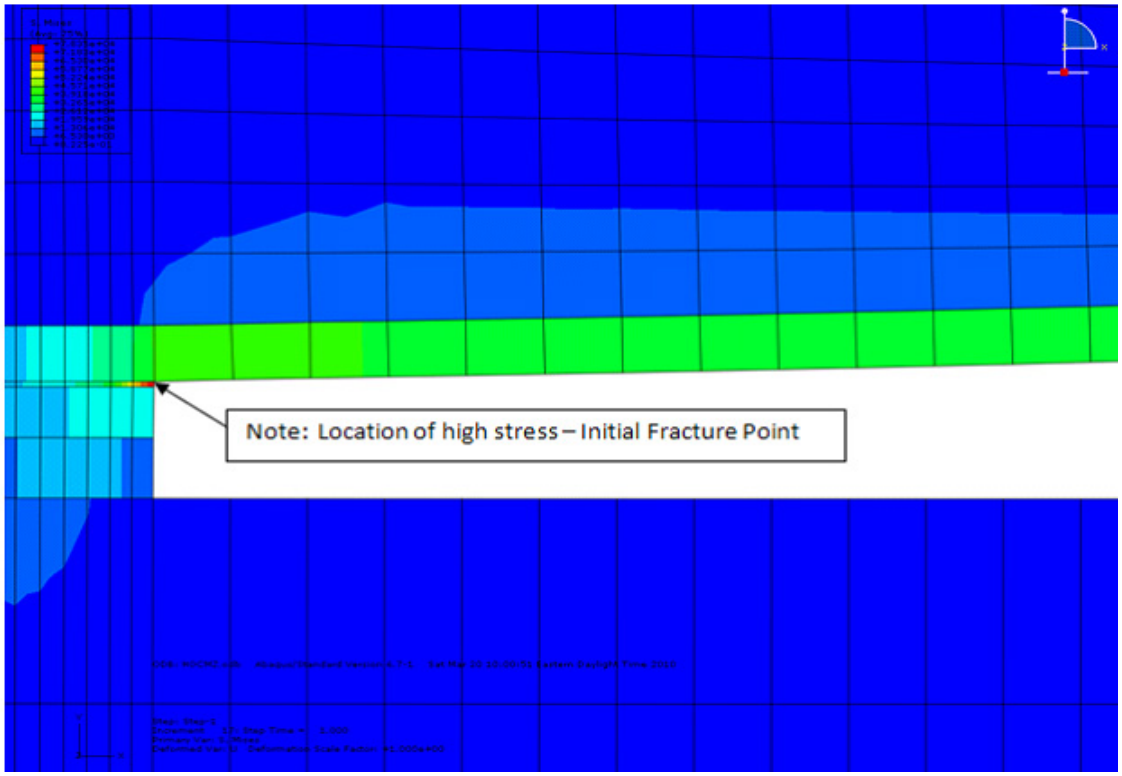

Figure 3.10 Stress Distribution in the Non-Separation Model

Conclusions

The preceding work documents the effectiveness of modeling the delamination of CFRP that has been bonded to concrete utilizing the Abaqus® defined cohesive element. The model does accurately predict the critical load, P_c as well as the crack opening displacement, *COD*. Furthermore, without the use of the cohesive element, the stress distribution at the crack initiation cannot be modeled properly. The significance of the numerical modeling is the accurate portrayal of the debonding process of SCCB test method with SP3 surface: as was the case with the experiment results, the model bears out the deep penetration into the concrete substrate. Comparing to the non-separation model (without cohesive element), the peak stress is significantly higher than the actual experimental results and the FRP material does not appear to resist the pull loading.

There are a few areas need to be addressed to fully define the SCCB analytically:

1. As multiple materials are contributing to the strength of the bond, it would be intuitive that each of these materials could be represented by multiple cohesive layers.
2. One area of concern is the added concrete material to the contour during fracture. The addition of this material could impact the compliance.
3. The non-homogeneity of the wood and concrete caused some concern when comparing the numerical results to the laboratory results.

CHAPTER 4: MODE I FATIGUE OF THE CFRP TO CONCRETE INTERFACE BOND

Submitted to the *Journal of Experimental Techniques*

Thomas Nicholas, UNCC, Shenen Chen, UNCC and David M. Boyajian Taylor Univ.

MODE I FATIGUE OF THE CFRP- CONCRETE INTERFACE BOND

ABSTRACT

The primary focus of the current research is to better define the behavior of the bonded interface region between the externally reinforcing CFRP composite member and the underlying concrete structure. While there has been more research performed on the fracture of this bonded region, a dearth remains on the phenomenon due to mechanical fatigue. This study utilizes the SCCB testing methodology to determine the fatigue life of the concrete to CFRP-concrete interface bond as subjected to mechanical cyclic loading. The specimens were subjected to a five hertz cyclic load under a load ratio of 50 percent. These research efforts made it possible to write a modified Paris law relationship for the CFRP-concrete interface bond as a predictive means of ascertaining the expected mechanical life cycle of such externally reinforced structures.

KEYWORDS: concrete repair; concrete strengthening; fiber reinforced polymer; modified Paris law; fatigue

---

Introduction

Carbon Fiber Reinforced Plastic (CFRP) has been recommended as a repair technique for concrete structures with the intent to strengthen the repaired structure (ACI, 2005). The success of actual strengthening is critically dependent on the quality of the bonding between the two materials. The primary focus of the current study is to investigate the fatigue behavior of the bonded interface between the externally reinforcing CFRP composite member and the underlying concrete under Mode I failure. The concrete was treated to the International Concrete Repair Institute (ICRI) surface profile three (SP3) as specified by the epoxy manufacturer, Sika® (2010). While much research has been performed on the fracture of the interface bonding between concrete and CFRP, a dearth remains on the performance due to mechanical fatigue.

This study utilizes the SCCB (Single Contoured Cantilever Beam) testing method (Boyaian, 2002) to determine the fatigue life of the concrete to CFRP-concrete interface bond as subjected to mechanical cyclic loading. Figure 4.1 shows the SCCB test setup, the technique is developed to confine the failure mode to Mode I fracture alone. The specimens were subjected to a five hertz cyclic load under a load ratio of 50 percent. The research outcome made it possible to establish a modified Paris law relationship for the CFRP-concrete interface bond as a predictive means of ascertaining the expected mechanical life cycle of such externally reinforced structures.

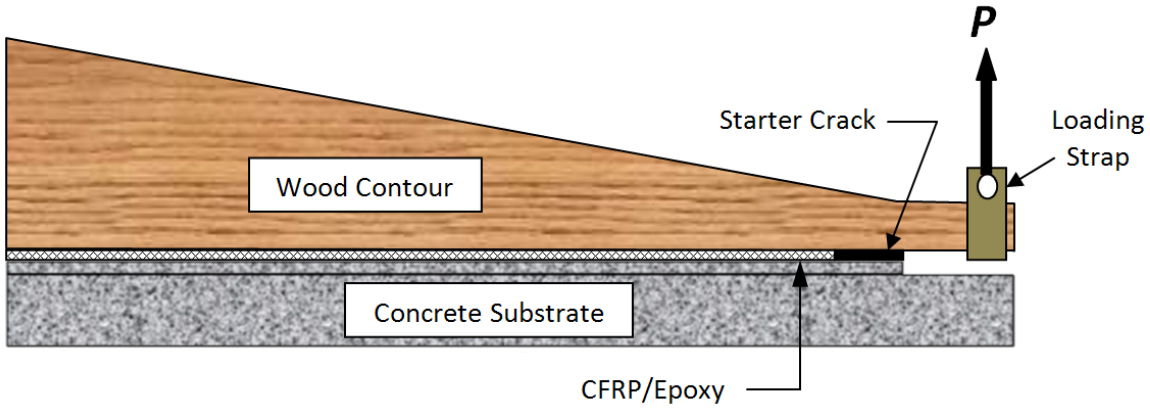

Figure 4.1 Side view of SCCB test (After Boyajian, 2002)

Lawrence and Boyajian (2006) provided a preliminary glimpse as to the behavior of the interface bond due to cycle loading; however, the scope of the work stopped at preliminary load ratios and frequency effects on fatigue life. Drawing from similar past research (Sebastain, 2001; Jia, 2002; Aidoo et al., 2004; and Ferrier, et al., 2005), the primary objectives of most fatigue studies is to provide a predictive model for fatigue life utilizing the power law (or Paris law) (Paris, et al., 1961; Paris and Erdogan, 1963) . The formula in its original form is given as:

$$\frac{\mathrm{d}a}{\mathrm{d}N} = C\Delta K^m \tag{4-1}$$

where

$\frac{\mathrm{d}a}{\mathrm{d}N}$ = crack growth rate (mm/cycle)

C = empirical material constant

ΔK = stress intensity factor

m = empirical material constant

Fatigue Life

Figure 4.2 shows a typical fatigue crack growth curve, where the three stages of the sigmoidal fatigue failure are: the threshold region (Region I), the intermediate region (Region II) and the critical or high growth rate region (Region III). The logarithmic

crack growth rate (da/dN) is plotted against a logarithmic function of the stress intensity factor, ΔK. The first region, near-threshold, provides little production as it pertains to crack growth rate. In Region I, the average crack growth is less than 10^{-6} mm/cycle and is often assumed to be zero (Dowling, 2000). In this region, the stress intensity range approaches the crack growth threshold, ΔK_{th}, which is the limit where the crack growth becomes measureable. The intermediate region (Region II) represents the majority of the usefulness for fatigue life of the structure and is the region represented by the power law. Crack growth in Region II is relatively linear in relation to stress intensity with the slope being characteristic of the material dependant variable, m. In the final stage (high growth stage), the stress intensity increases at a high rate until reaching the critical value, K_c. Once the critical stress intensity is achieved, the material experiences catastrophic failure. Table 4.1 lists the material constants for fatigue fracture in concrete (Li and Matsumoto, 1998) and wood/FRP interface(Jia et al., 2005). Notes from Table 4.1 also indicated that the Paris law presented as either a function of crack tip stress intensity factor or the average strain energy release rate, which is discussed below.

Table 4.1 Paris Law Constants

Material	B	m	Notes
Plain Concrete	9.03×10^{-6}	3.12	Paris Law in crack tip stress intensity factor amplitude (Li and Matasumoto, 1998)
Concrete (FRP Bars)	7.51×10^{-5}	3.76	Paris Law in critical strain energy release rate(Zhou, 2004)
Wood /FRP Mode I	5×10^{-5}	5.77	Paris Law in critical strain energy release rate(Jia, et al., 2005)
Concrete/FRP Mode I (current study)	2×10^{-8}	2.997	Paris Law in critical strain energy release rate

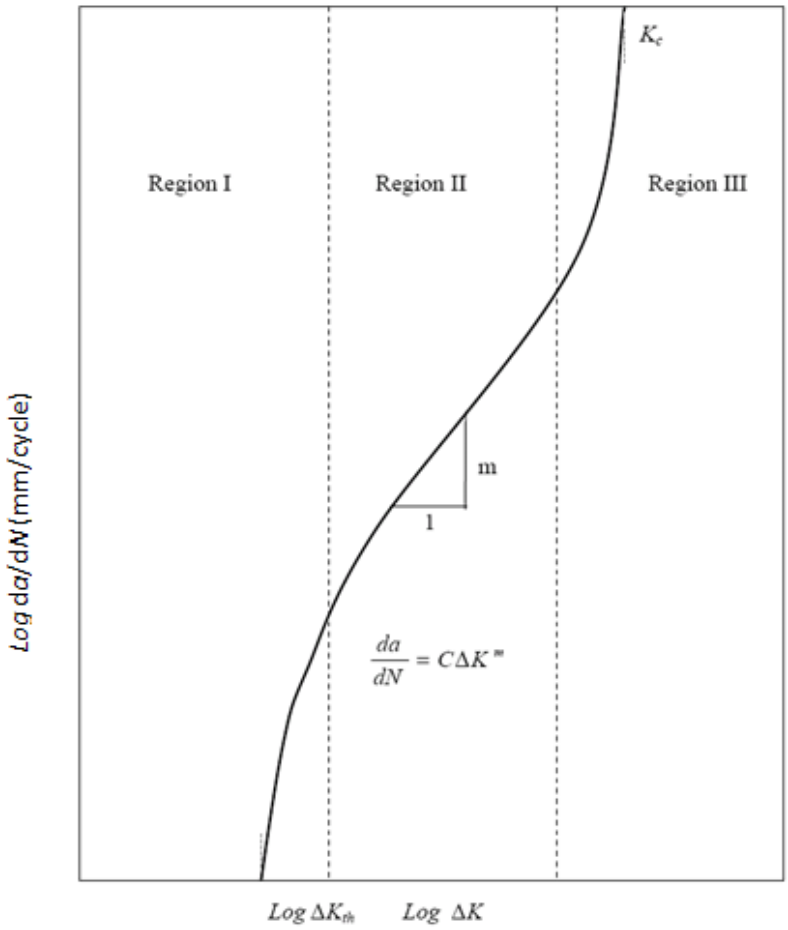

Figure 4.2 Three Stages of the Fatigue Process (after Suresh, 1998)

The CFRP to concrete interface bond, hypothetically, is a combination of two materials, the carbon fiber reinforced polymer composite and the concrete. While no previous studies specifically targeted this particular combination of materials, a number of past researchers have developed modified Paris law equations for other bonded materials, where the stress intensity factor is replaced by the strain energy release rate. The modified Paris Law equation from Sutton (1974) for bonded materials is as:

$$\frac{\mathrm{d}a}{\mathrm{d}N} = B(\Delta G)^m \tag{4-2}$$

where $\frac{da}{dN}$ = crack growth rate(mm/cycle)

B = empirical material constant

ΔG = average strain energy release rate range (J/m^2)

m = empirical material constant

The commonly accepted method for representing fracture toughness is the critical strain energy release rate, G_C, as defined by the Irwin-Kies (1954):

$$G_C = \left(\frac{P_C^{\,2}}{2b}\right)\left(\frac{dC}{da}\right) \tag{4-3}$$

where: G_C = Critical strain energy release rate (J/m^2)

P_C = Critical load (N)

b = width of the specimen (mm)

dC/da = Rate of compliance (C) to crack length (a) (N^{-1})

ΔG can then be calculated as follows:

$$G_{C-\max} = \left(\frac{P_{C-\max}^{\,2}}{2b}\right)\left(\frac{dC}{da}\right) \tag{4-4}$$

$$G_{C-\min} = \left(\frac{P_{C-\min}^{\,2}}{2b}\right)\left(\frac{dC}{da}\right) \tag{4-5}$$

and

$$\Delta G = G_{c\text{-}max} - G_{c\text{-}min} \tag{4-6}$$

where $P_{c\text{-}max}$ = maximum fatigue load

$P_{c\text{-}min}$ = minimum fatigue load

The following relationship has been proposed to calculate the crack growth rate (Jia, et al., 2005):

$$\frac{da}{dN} = \frac{da}{dC}\frac{dC}{dN} = \frac{1}{kP}\frac{dCOD}{dN} \tag{4-7}$$

where P = applied load (N)

k = compliance gradient

$\frac{dCOD}{dN}$ = crack opening displacement propagation rate (mm/cycle)

In order to define the material constants, B and m, the values for da/dN and ΔG must first be determined. Following the modified Paris law (Equation 4-2), the crack propagation rate is presented as a function of the average critical strain energy release rate which is readily calculated by Equation 4-6. Since the SCCB test specimen was utilized (crack growth is not directly measured) for the testing methodology, the crack growth rate had to be related to the compliance gradient in order to compute the crack propagation rate. This can be readily found using Equation 4-7.

Fracture of FRP Bonded to Concrete

Concrete structural members that have been strengthened by wet layup FRP systems can fail due to different debonding mechanisms as illustrated in Figure 4.3. As the figure shows, the system can debond in several ways including FRP delamination, interface failure, concrete substrate failure, and rebar delamination. Due to this limitation of the strengthening system, it is imperative to develop a strong enough bond that forces the failure to occur in the concrete substrate. Chapter 2 of this study presented the relationship that utilizing a standard mix design and the Surface Profile 3 (SP 3) the fracture readily propagated in the concrete substrate. The study was validated through normalizing a previous work by Boyajian (2002) (Figure 4.4). It should be noted that both studies produced failure in the substrate material.

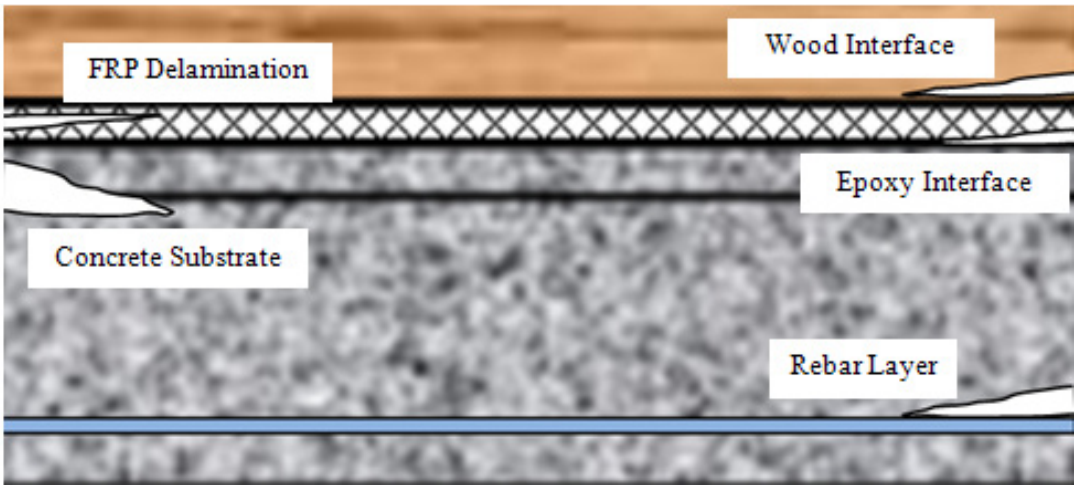

Figure 4.3 Types of Debonding for SCCB Test Specimen.

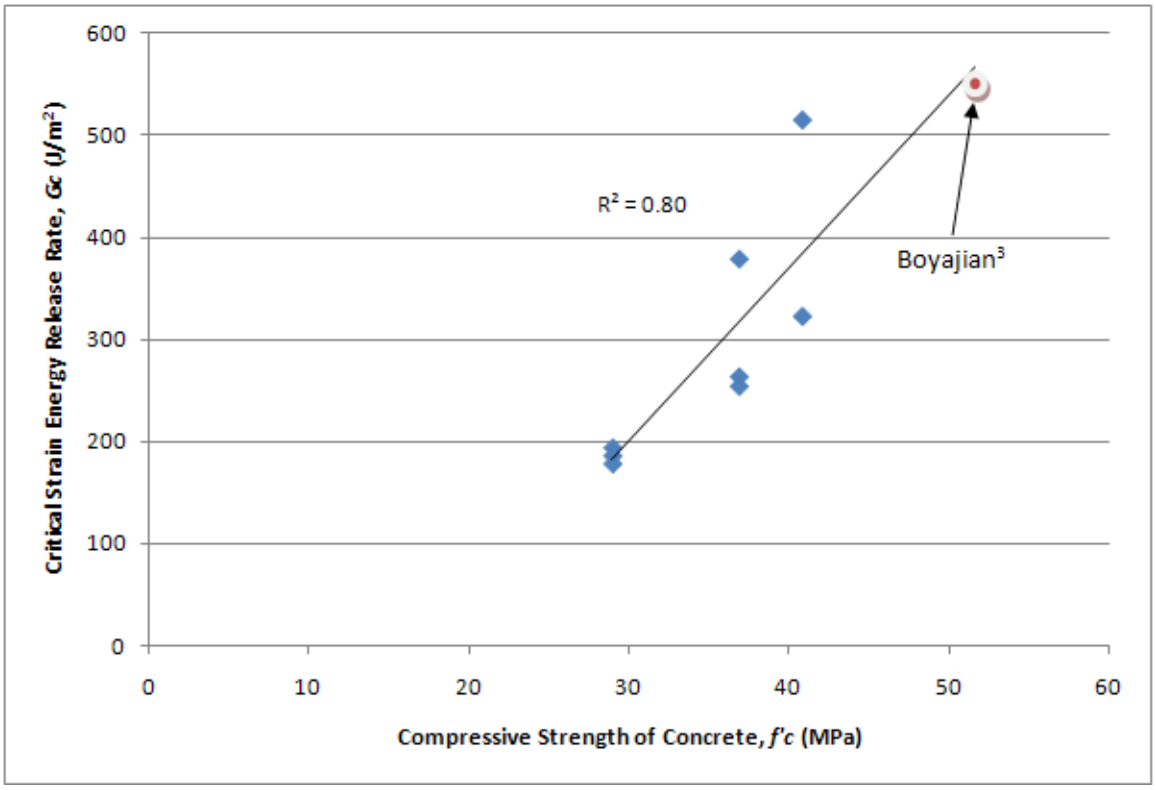

Figure 4.4 Average Critical Strain Energy Release Rate as a Function of Concrete Compressive Strength with Boyajian (2002) Averaged Data Included.

Determining the critical load, P_c, is integral to the fatigue process, in that, the window of applied loads for the fatigue test is directly determined from the fracture tests. If the initial fatigue load is too high, then cyclic loading will not occur with ensuing fracture failure. Conversely, if the initial fatigue load is too low, failure may not be achieved in a reasonable amount of cycles. The beginning fatigue load for this study was taken as 65 percent of the fracture load determined from tests done in Chapter 2.

EXPERIMENT

SCCB Material

The single cantilever contoured beam (SCCB) used for this study is comprised of a substrate material (reinforced concrete), a fiber reinforced polymer layer and a wood contour as illustrated in Figure 4.1. The substrate was normal weight concrete with a target compressive strength of 41.4 MPa. The contour material used in the study is a wood product, 1.9E Microllam® LVL (Laminated Veneer Lumber) manufactured by Weyerhaeuser. Additionally, the FRP system selected for the study was Sikadur® 301 two-part epoxy and SikaWrap® Hex 103C carbon fiber. Static fracture tests were conducted to determine the peak failure loads for the specimen. Figure 4 shows the computed values critical strain release rates (G_C) from the fracture tests, which are confirmed by previous data completed on different surface treatments (Boyajian, 2002).

Fatigue Test

For the foundational work of fatigue of the bonded interface using the SCCB, four SCCB specimens will be used to determine the fatigue life of the bond by developing the modified Paris Law. A frequency of five hertz was selected as the baseline due to most engineering structures experience frequencies of one to five hertz over a 120 year life

span (Ferrier, et al., 2005). A frequency of one hertz is referred to as a low fatigue life and five hertz is labeled as middle fatigue life(Zhang and Wu, 1997). While load ratio will have an effect on the fatigue life of the bonded interface, R = 0.5, was selected to provide mid level values (e.g. R: 0 → 1).

The testing regimen consisted of placing the SCCB specimens in the 20-Kip MTS® machine and submitting them to the described cyclic loading until interface failure was achieved (Figure 4.5). The initial maximum and minimum loads were determined based on 65 percent of the fracture critical load (from fracture test) and a load ratio, R = 0.5, respectively. For example, given the critical load of 1,557 N, the initial maximum load would be 1,010 N and the minimum would be 50 percent of the maximum load = 507 N. For ease of calculation and record keeping, these values were rounded to the nearest 111 N, as listed in Table 4.2. The final percentage for maximum and minimum loads was closer to 80 percent according to the test results. For each maximum and minimum load (fatigue test), the total number of cycles, N, was plotted as a function of COD as illustrated by Figure 4.6.

Table 4.2 Fatigue Results

Pmax (N)	*Pmin (N)*	*Gmax* (J/m^2)	*Gmin* (J/m^2)	*ΔG* (J/m^2)	d*a*/d*C* (N^{-1})	d*COD*/d*N* (mm/cycle)	d*a*/d*N*
1335	667.5	584.21	146.0533	438.1600	1.49E-05	2.00E-08	1.01E-06
1112	556	405.34	101.3348	304.0043	1.49E-05	5.00E-09	3.02E-07
1045	522.5	357.97	89.4914	268.4743	1.49E-05	8.00E-09	5.14E-07
890	445	259.65	64.9126	194.7378	1.49E-05	1.00E-09	7.54E-08

Figure 4.5 Single Contoured Cantilever Beam Fracture Test in the 20-kip MTS Machine®

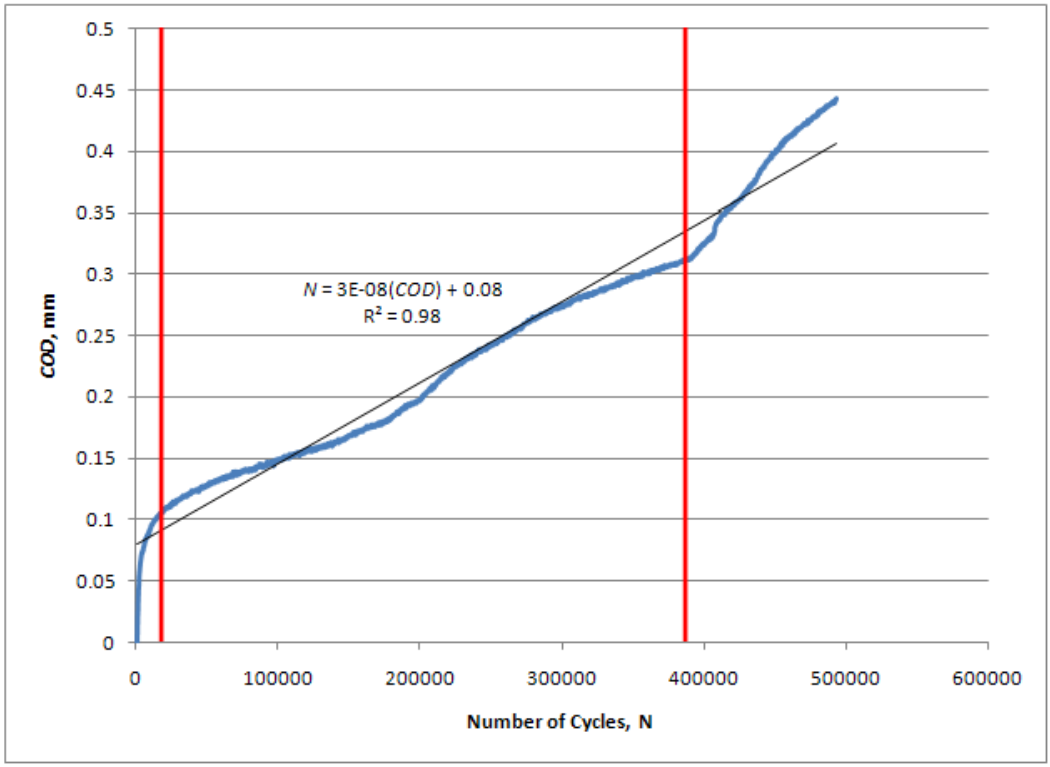

Figure 4.6 COD Versus Number of Cycles for a SCCB Specimen Under 667-1,334 N Cyclic Loading with a Frequency f = 5 Hz, Load Ratio R = 0.5 and Sinusoidal Waveform

Test Results

Table 4.2 shows the computed da/dN and strain energy rate, ΔG. As previously presented, the majority of the fatigue life presents itself in Region II. It was necessary to define a point to where failure of the system was achieved as well as ensuring that Region II fatigue life was properly defined. For the current study, the failure was linked to fracture results through the crack length of 152 mm (one third the specimen length), the fracture is assumed to reach the critical load. As can be seen in Figure 4, the SCCB was tested until all three stages of fatigue life were achieved. The linear region is bounded by the two red lines with that data being utilized to determine the resulting dCOD/dN value of 2.0E-8. The failure of the interface for the SCCB specimens occurred much closer to

the FRP layer than with fractured specimens. As shown in Figure 4.7, while the interface resides predominantly in the concrete, there is a mixture of epoxy, FRP and concrete on the face of the failed plane. Figure 4.7(b) illustrates a close-up view of the failed specimen. This common failure type was experienced by all the cyclic loaded specimens.

a) Fatigue Failed Specimen

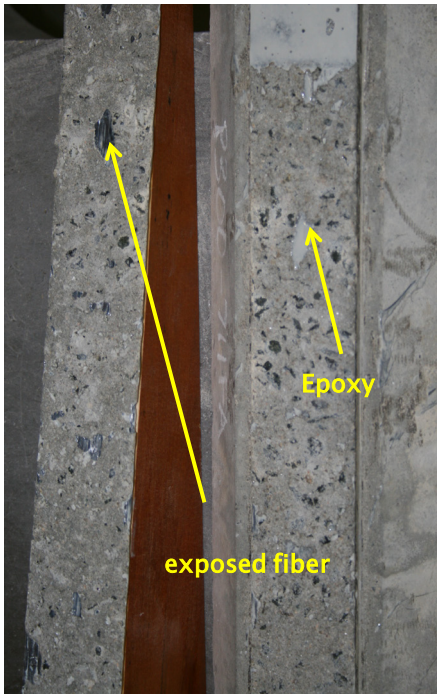

b) Close-Up of Failed Fatigue Specimen, the failure plane is closer to the CFRP as evidenced by the patches of visible fibers. Also, the bright white areas are epoxy failures.

Figure 4.7 Failed Fatigue Specimen (a) Concrete Base and CFRP Strip; b) Exposed Substrate, Fibers and Epoxy)

The resulting linear regression in Figure 4.8 (as well as Figure 4.6) provides as an example in determining the d*COD*/d*N* value. At this point, the crack growth rate can be calculated and then plotted as a function of ΔG, as illustrated by Figure 4.9. The results for ΔG and d*a*/d*N* are listed in Table 4.2. To develop the modified Paris law, d*a*/d*N* is

plotted as a function of ΔG on a log-log scale and an exponential regression is created accordingly. From the regression, B and m can be determined. For this study, $B = 2 \times 10^{-8}$ and $m = 3$. Therefore, the modified Paris law relationship for the 5 Hz and 0.5 load ratio case can be written as:

$$\frac{da}{dN} = 2 \times 10^{-8}(\Delta G)^3 \tag{4-8}$$

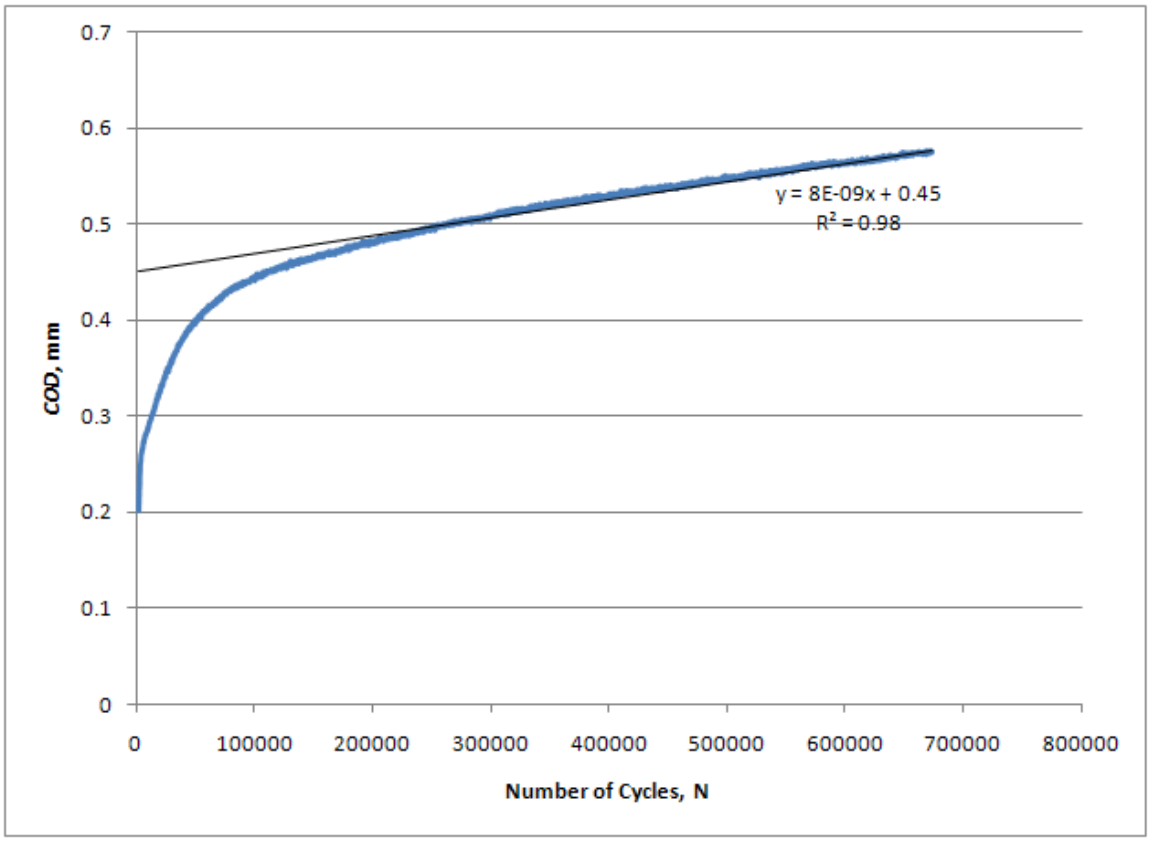

Figure 4.8 COD Versus Number of Cycles for a SCCB Specimen Under 523 – 1,045 N Cyclic Loading with a Frequency f = 5 Hz, Load Ratio R = 0.5 and Sinusoidal Waveform

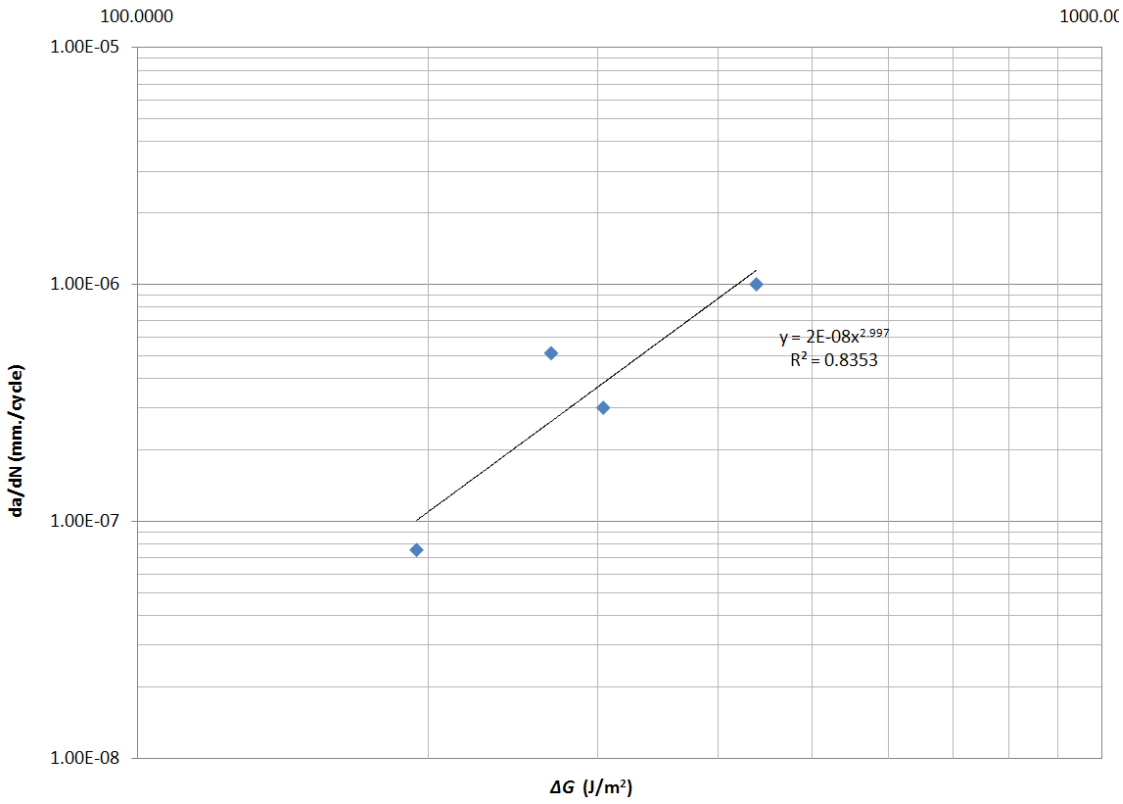

Figure 4.9 *Log-Log* Plot of Crack Growth Rate as a Function of Strain Energy Release Rate

Conclusions

The study illustrates that the SCCB is a viable system for determining fatigue life of the reinforced concrete to CFRP bond interface as it pertains to developing the modified Paris law. Four SCCB samples were tested to a prescribed failure of one third the length and the corresponding d*a*/d*N* and Δ*G* values calculated. From these values, the material properties, *B* and *m*, were determined based on the exponential regression of the d*a*/d*N* and Δ*G* plot. Interestingly, the failure of the concrete to CFRP interface was shallower than the failure plane of the fractured specimens and contained areas of epoxy and concrete. It should be noted, however, that while this is a significant step towards

developing the modified Paris equation; the load ratio will have an effect on the final modified equation and needs to be investigated.

As is pertains to test methodology, the study also found that a beginning fatigue load of 80 percent, instead of 65 percent, was a more realistic starting load. For future studies, the surface of the concrete substrate at the initial crack tip location should be studied at the micro level.

CHAPTER 5: CONCLUSIONS AND FUTURE DIRECTIONS

5.1 Conclusions

The overreaching goal of this study was to better define the behavior of the CFRP to concrete bonded interface. This was accomplished through treating the surface of the concrete to ICRI surface profile SP 3 standards, developing a finite element model of the SCCB system, and subjecting the specimens to Mode I fracture and fatigue. The major difference between the various SCCB studies and the current study was the use of the SP 3 surface profile. While Lawrence and Boyajian (2006) did investigate the impact of different surfaces to bond strength, none of the surfaces achieved the level of SP 3 as defined by ICRI. However, the work did highlight that surfaces with rougher profiles produced higher bond strengths.

The preliminary hypothesis is, of course, the surface profile aids in producing a bond strength that far exceeds the strength of the concrete substrate. This is evidenced by the cohesive failure located entirely in the concrete substrate and therefore, the fracture energy would primarily be a function of the fracture energy of concrete. However, a review of studies performed by Moavenzadeh and Kuguel (1969); Kaplan (1961); Brown (1972); and Jenq and Shah (1985) showed that the fracture energy of concrete from the current study is significantly higher than their reported values. The only conclusion can be that even with the deep penetration into the concrete substrate, there exists a

contribution from the CFRP system, or interface region. The following summarizes the contributions of the preceding work:

- The current work found that for normal strength concrete, an increase in compressive strength correlates to an increase in the critical strain energy release rate when all data points are plotted with a confidence of R^2 = 0.79. Additionally, when the critical strain energy release rate is averaged for each compressive strength, the confidence raised to $R^2 = 0.88$.
- The results of the current finite element analysis illustrates that the cohesive element is a viable option in modeling the SCCB. The model does accurately predict the critical load, P_c as well as the crack opening displacement, *COD* for averaged material values. Of other significance, as was the case in the lab, the model bears out the deep stress penetration into the concrete substrate for the pristine specimens.
- The study also illustrates that the SCCB is a viable system for determining fatigue life of the reinforced concrete to CFRP bond interface as it pertains to developing the modified Paris law. Four SCCB specimens were tested to a prescribed failure of one third the length and the corresponding d*a*/d*N* and ΔG values calculated. From these values, the material properties, *B* and *m*, were determined based on the exponential regression of the d*a*/d*N* and ΔG plot. The modified Paris law was then developed for the standard 1:3:5 mix design and FRP system as follows:

$$\frac{\mathrm{d}a}{\mathrm{d}N} = 2 \times 10^{-8}(\Delta G)^3$$

Interestingly, the failure of the concrete to CFRP interface was shallower than the failure plane of the fractured specimens and contained areas of epoxy and concrete. This would further the argument that the SCCB is a viable option for testing the interfacial qualities of the bonded system. It should be noted, however, that while this is a significant step towards developing the modified Paris equation; the load ratio will have an effect on the final modified equation.

5.2 Future Directions

- In interpreting the fracture results, regardless of the compressive strength of the substrate, the crack growth pattern among the specimens was similar in that they experienced the deep intrusion into the substrate. This deep substrate failure was not readily experienced in previous SCCB studies and therefore determining its cause should become a focus of future analytical studies.
- While this study confirms that the bond strength of pristine concrete to CFRP specimens is a function of substrate compressive strength, only normal concrete, i.e. f'_c < 41.40 MPa has been tested. Further testing would be required for bond behavior of high strength concretes. The behavior of the bond due to the ICRI SP 3 surface should be further investigated for high performance concrete as well. Furthermore, fracture studies of the ICRI surface profile should be performed for specimens that

have been subjected to freeze-thaw cycles and wet-dry cycles for both normal concrete and high performance concrete.

- As multiple materials are contributing to the strength of the bond, it would be intuitive that each of these materials could be represented by multiple cohesive layers in the finite element model. Current models are underway to investigate this possibility. One area of concern raised by the finite element analysis is the added concrete material to the contour during fracture. The addition of this material could be impacting compliance and further investigation is warranted. The non-homogenous nature of the wood and concrete causes some concern when comparing the numerical results to the laboratory results and therefore, further material analysis and effects should be studied.
- The effects of surface preparation on the fatigue life of the concrete to CFRP interface should be determined. As with the fracture, the failure plane was readily found to be primarily in the concrete substrate. The load ratio effect should be quantified for the SCCB system and the corresponding modified Paris Law developed. A finite element model of the SCCB system subjected to cyclic loading should be developed to assist in determining the bonded interface behavior.
- The newer Microllam® LVL, while a fine product, cannot be utilized for the SCCB. This would pose a problem for future studies given that the original Microllam® LVL is no longer available. The use of Plexiglas should be studied as a viable alternative for the SCCB testing system. The

SP 3 surface profile still produced a bond that was stronger than the interface causing material failure and not bond failure. However, it is hypothesized that the SP 3 surface profile produces an inconsistent surface at the micro-level and is a driving factor in the variability of the fatigue results

- Referring to Appendix B, the fracture results of the weathered specimens show that the interface region behaves in a much more brittle manner than the pristine specimens of the earlier study which was expected due to the findings of Shahrooz et al. (2003). In Shahrooz's study, it was determined that CFRP fabrics/epoxy systems became brittle during the freeze-thaw cycling period.
- Of further importance is the location of the fracture plane for the weathered specimens. As previously stated, the wet conditions of freeze/thaw (Abanilla et al., 2005) should result in some degradation of the epoxy. However, while the failure was shallower in nature, e.g. closer to the bonded area than with the pristine specimens, the epoxy bond proved to still be stronger than the damaged concrete. The result of the material failure is still a cohesive failure instead of the expected adhesive failure reported by Davalos et al. (2008) and Boyajian (2002).
- The behavior of the SP 3 surface profile is inconsistent as it pertains to durability testing of fatigue. The number of run-out tests suggests that the critical fatigue load is not being achieved. As a way to better define the critical fatigue load, a sample run-out specimen was fractured to determine

exactly what was causing the inconsistencies. Using specimen FT300_1030_04, a critical strain energy fracture test was performed with a result of 823 N – 243 MPa greater than the baseline specimens.

REFERENCES

Abanilla, M.A., Li, Y., Karbhari, V.M., (2005) "Durability characterization of wet layup graphite/epoxy composites used in external strengthening," *Composites*, Part B Vol. 37, pp. 200–212

ABAQUS Finite Element Code (2007), Hibbit, Karlsson and Sorensen, Inc., RI.

ACI 301-05, (2005) "Specifications for Structural Concrete," American Concrete Institutem, ACI Committee 301, technical committee document, 49 pp.

ACI 440.2R-08, (2008) "Guide for the design and construction of externally bonded FRP systems for strengthening concrete structures," American Concrete Institute.

Aidoo, J., Harries, K.A. and M.F. Petrou, (2004) "Fatigue of Large-Scale Reinforced Concrete T-Beams Strengthened by FRP Composites", *ASCE Journal of Composites for Construction*, Vol. 8, No. 6, pp. 501-509.

ASTM C666-97, (1997) "Standard test method for resistance of concrete to rapid freezing," American Society for Testing and Materials.

ASTM C672/C672M-98 (1998) "Standard test method for scaling resistance of concrete surfaces exposed to deicing chemicals", American Society for Testing & Materials.

Bazant, Zdenek P. and Planas, Jaime. (1998) *Fracture and Size Effect in Concrete and other Quasibrittle Materials*, CRC Press LLC, Boca Raton, FL, 616 pp.

Berry, J.P. (1963) "Determination of Fracture Surface Energies by the Cleavage Technique," *J. of Applied Physics*, Vol. 34, No.1, pp. 62-68.

Boresi, Arthur, Schmidt, Richard J. and Sidebottom, Omar M. (1993) *Advanced Mechanics of Material*, John Wiley & Sons, Inc., New York, NY, Fifth Edition, 811 pp.

Boyajian, D.M., Davalos, J.F. and Ray, I. (2005) "Freeze-thaw cycling under a calcium chloride environment: effects on CFRP strengthened concrete structures", *International Journal of Materials and Products*, Vol. 28, No. 1/2, pp.89-102.

Boyajian, D.M.,J.F.Davalos and I.Ray (2002) *Evaluation of Interface Fracture of Concrete Externally Reinforced with FRP*. in Proceeding's The Second international Conference on Durability of Fiber Reinforced Polymer (FRP) Composites for Construction (CDCC). Montreal, Quebec, Canada.

Boyajian, D.M.,J.F.Davalos and I.Ray (2002) *Evaluation of Interface Fracture of Concrete Externally Reinforced with FRP*. in Proceeding's The Second international Conference on Durability of Fiber Reinforced Polymer (FRP) Composites for Construction (CDCC). Montreal, Quebec, Canada.

Boyajian, David M., (2002). Mode I Fracture and Durability of the CFRP-Concrete Interface Bond, Ph.D. Dissertation, West Virginia

Boyajian, David M., Davalos, Julio F. and Qiao, P. (2000) "Development of a Test Specimen for FRP-Concrete Mode-I Fracture," Proceedings of the Third International Conference on Advanced Composite Materials in Bridges and Structures (ACMBS), Ottawa, Canada, August 15-18, 2000, J.L. Humar and A.G. Razaqpur (editors), pp.445-452.

Brown, J.H., (1972) "Measuring the fracture toughness of cement paste and mortar," *Magazine of Concrete Research* 24(81) 185-196.

Buyukozturk, O., Gunes, O. and karaca, E., (2004) "Progress on Understanding Debonding Problems in Reinforced Concrete and Steel members Strengthened Using FRP Composites," Construction and Building Materials, Vol.18, pp. 9-19.

Carlsson, Leif A. and Pipes, Byron R. (1987) *Experimental Characterization of Advanced Composite Materials*, Prentice-Hall, Inc., Englewood Cliffs, NJ, pp. 197.

Cordon, W.A. (1967) *Freezing and Thawing of Concrete.Mechanisms and Control*, American Concrete Institute/Iowa State University Press, Monograph No. 3, second printing, Detroit, Michigan, pp.99.

Davalos, J. F., Kodkani, S. S., Ray, I. and Lin, C., (2008) "Fracture Evaluation of GFRP-Concrete Interfaces for Freeze-Thaw and Wet-Dry Cycling," *Journal of Composite Materials*; Vol. 42.

Diehl, T., (2008) "*On using a penalty-based cohesive-zone finite element approach, Part I: Elastic solution benchmarks*," International Journal of Adhesion & Adhesives, Vol. 28, pp. 237–255.

Dowling, N. E., and Thangjithan, S., (2000) "An Overview and Discussion of Basic Methodology for Fatigue," Fatigue and Fracture Mechanics: 31st Volume, ASTM STP 1389, G. R. Halford and J. P. Gallagher, Eds., American Society for Testing and Materials, West Conshohocken, PA, pp. 3-36.

Duan K, Hu XZ, Wittmann FH. (2007) "Size effect on specific fracture energy of concrete," Engineering Fracture Mechanics; Vol. 70, pp. 87−96.

Ferrier, E., Bigaud, D., Hamelin, P., Bizindavyi, L., and Neale, K.W., (2005) "Fatigue of CFRPs Externally Bonded to Concrete," *Materials and Science*, Vol. 38, January-February, pp. 39-46.

Giurgiutiu, V., J.Lyons, M.Petrou, D.Laub and S.Whitley (2001), *Fracture Mechanics Testing of the Bond Between Composite Overlays and a Concrete Substrate.* Journal of Adhesion Science and Technology, Vol. 15, No. 11: pp. 1351-1371.

Hertzberg, Richard W. (1976) *Deformation and Fracture Mechanics of Engineering Materials*, John Wiley & Sons, New York, NY, 605 pp.

Huang, D. and Lyons, J., (2005) "*Finite Element Analysis of Test Specimens to Assess Composite–Concrete Bond Durability*," Journal of Reinforced Plastics and Composites, Vol. 24, pp. 1387 – 1406.

International Concrete Repair Institute, (2003) "Concrete Surface Preparation for Fiber Reinforced Polymers." Des Plains, IL

Irwin, G.R. (1958) "Fracture," *Encyclopedia of Physics*, Ed. S. Flugge, Springer, Berlin, Vol. VI, pp. 551-590.

Irwin, G.R. and Kies, J.A. (1954) "Critical Energy Rate Analysis of Fracture Strength," The Welding Journal, Research Supplement, Vol. 33, pp. 193-198.

Jenq, Y.S. and Shah, S.P., (1985) "A fracture toughness criterion for concrete," *Engineering Fracture Mechanics* Vol. 21, No. 5, pp. 1055-1069.

Jia, J., (2002) "Mode-I Fatigue Fracture of Interface for Fiber-Reinforced Polymer Composite Bonded to Wood," Doctoral Dissertation, West Virginia University.

Jia, J., Boothby, T.E., Bakis, C.E., and Brown, T.L. (2005) "Durability Evaluation of Glass Fiber Reinforced-Polymer-Concrete Bonded Interfaces," *Journal of Composites for Construction*," ASCE Vol. 9, No. 4.

Kabhari, C. (2005) "A Fracture Mechanics Approach To Assessment of Defect Criticality in FRP Rehabilitated Concrete," Appendix 2 of A Fracture Mechanics to Assessment of Defect Criticality in FRP Rehabilitated Concrete_Appendix 2 of Oregon DOT Report.

Kaplan, M.F., (1961) "Crack propagation and the fracture of concrete," *J. American Concrete lnstitute* Vol. 58, No. 5, pp. 591-610.

Karbhari, V. M., Rivera, J. and Dutta, P. K. (2000) "Effect of Short-Term Freeze-Thaw Cycling on Composite Confined Concrete," *Journal of Composites for Construction*, Vol. 4, pp. 191-197

Karbhari, V.M. and M. Engineer (1996), *Investigation of Bond Between Concrete and Conposites: Use of a Peel Test.* Journal of Reinforced Plastics and Composites, Vol. 15 (February): pp. 208-227.

Kimpara, I., K.Kageyama, T.Suzuki, I.Osawa and K.Yamaguchi (1999), *Characterization of Debonding Energy Release Rate of FRP Sheets Bonded on Mortar and Concrete.* Advanced Composite Materials, Vol. 8, No. 2: pp. 177-187.

Kodkani, Shilpa Sudhir (2004). Interface Durability of Externally Bonded GFRP to Normal and High-Performance Concrete, Master's Thesis, West Virginia University, [On-line Abstract]. https://eidr.wvu.edu/etd/documentdata.eTD?documentid=3601

Lawrence, Timothy O., and Boyajian, David M., (2006) "Surface Roughness, Quasi-Static Fracture, and Cyclic Fatigue Effects on GFRP- and CFRP-Concrete Bonded Interfaces," *Journal of ASTM International*, Vol. 3, No. 1, pp. 1-14.

Li, V. C. and Matsumoto, T., (1998) "Fatigue Crack Growth Analysis of Fiber Reinforced Concrete with Effect of Interfacial Bond Degradation," *Cement and Concrete Composites*, Vol. 20, pp. 339-351.

Liu-Nash, G., Todd, J. A. and Mostovoy, S. (1997) "An Accelerated Test Method for Determination Near-Threshold Stress Intensity Values in HSLA Steels," Fatigue Fract. Engng. Mater. Struct. Vol. 20, No. 12, pp. 1657-1664.

Moavenzadeh, F. and Kuguel, R., (1969) "Fracture of concrete," *Journal of Materials* 4(3) 497-519.

Mohamed, O. A., Rens, K. L., and Stalnaker, J. J., (2000) "Factors Affecting Resistance of Concrete to Freezing and Thawing Damage" Journal of Materials in Civil Engineering Vol.12, No.26.

Mostovoy, S., and Ripling, E. J., (1975) "Flaw Tolerance of a Number of Commercial and Experimental Adhesives," Polymer Science Technology B, Vol. 9B, pp. 513-562.

Mostovoy, Sheldon, Crosley, P.B. and Ripling, E.J. (1967) "Use of Crack-Line-Loaded Specimens for Measuring Plane-Strain Fracture Toughness," J. of Materials, Vol. 2, No. 3, pp. 661-681.

Paris, P. C. and Erdogan, F., (1963) "Critical Analysis of Propagation Laws," J. of Basic Engineering, Vol. 85, pp. 528-534.

Paris, P. C., Gomez, M. P. and Anderson, W. E., (1961) "Rational Analytical Theory of Fatigue," The Trend in Engineering, Vol. 13, No. 1, pp. 9-14.

Polakowski, N.H. and Ripling, E.J. (1966) *Strength and Structure of Engineering Materials*, Prentice-Hall, Inc., Englewood Cliffs, New Jersey, 535 pp.

Qiao, P. and Xu, Y. (2004) “Effects of Freeze-Thaw and Wet-Dry Conditions on the Mode I Fracture of FRP-Concrete Interface Bonds,” *Proceedings of Earth and Space 2004*, March 7-10.

River, Bryan H. (2002) "Fracture of Adhesive-Bonded Wood Joints," Handbook of Adhesive Technology, 2nd Ed., Eds. A. Pizzi and K.L. Mittal, Marcel Dekker Inc., New York, NY.

Sebastian, M. W. (2001) “Significance of Midspan Debonding Failure in FRP-Plated Concrete Beams”, *ASCE Journal of Structural Engineering*, Vol. 127, No.7, 792-798.

Shahrooz, B. M., Pack, J. R., Baseheart, T. M., Rieser, L. A., (2003) “Environmental Durability Evaluation OF Externally Bonded Composites,” Report No. UC-CII 03/02 Federal Highway Administration and Ohio Department of Transportation

Sika®, (2010) Sikadur® materials data sheet.

Suresh, S., (1998) Fatigue of Materials, Second Edition, Cambridge University Press, Cambridge, UK.

Sutton, A. S, (1974) “Fatigue Crack Propagation in an Epoxy Polymer,” Engineering Fracture Mechanics, Vol. 6, pp. 587-595.

Turon, A., Da´vila C.G., Camanho P.P., Costa J., (2007) “An engineering solution for mesh size effects in the simulation of delamination using cohesive zone models,” *Engineering Fracture Mechanics* Vol. 74, pp. 1665−1682

Zhang, B. and Wu, K. (1997) “Residual Fatigue Strength and Stiffness of Ordinary Concrete under Bending,” *Cement and Concrete Research*, Vol. 27, No. 1, pp. 115-126.

Zhou, Y. (2004) *FRP Reinforced Concrete and Its Application in Bridge Slab Design*, PhD Dissertation, Case Western University, Cleveland, Ohio.

APPENDIX A: CONCRETE MATERIALS

This section is a compilation of the concrete testing regimen and batch results.

Type of loading	Number	Type of loading	Number
CONDITIONED SPEC.		**CONDITIONED SPEC.**	
Fracture		Fracture	
100	3	20 week	4
200	3		
300	3	Fatigue	
Fatigue		20 week	4
100	3		
200	3	BASELINE	
300	3	Fracture	
BASELINE		20 week	3
Fracture			
100	3	Fatigue	
200	3		
300	3	20 week	3
Fatigue			
100	3		
200	3		
300	3		
TOTAL	36	TOTAL	14
Pristine	12		
TOTAL NUMBER OF SPECIMENS		62	

Concrete Substrate Mix Design

Job Weight Calculations:			Job Volume Calculations:		
For Job of:	0.05	m^3	For Job of:	0.05	m^3
Cement	25.59	kg	Cement	0.009	m^3
Coarse Aggregate	57.61	kg	Coarse Aggregate	0.02	m^3
Fine Aggregate	29.48	kg	Fine Aggregate	0.01	m^3
Water	10.89	kg	Water	0.01	m^3
Air	0	kg	Air	0.003	m^3
Air Entrainment	28.35	g	Air Entrainment	0.0	m^3
Water Reducer	0	g	Water Reducer	0.0	m^3

Concrete Batch Test Results

Pour	Air Content	Slump (mm)	No. of Beams	f'c (MPa)
Batch - 3/27	6.00%	76	18	40.85
Batch - 6/16	6.75%	95	18	28.95
Batch - 7/11	5.75%	89	18	38.38
Batch - 10/30	6.50%	102	18	37.92
Average	6.25%	91		36.55

APPENDIX B: BEHAVIOR OF THE BONDED INTERFACE SUBJECTED TO FREEZE/THAW ENVIRONMENT AND MODE I FRACTURE/FATIGUE UTILIZING THE SP3 SURFACE PROFILE

To be submitted as Part of a Future Research Proposal

BEHAVIOR OF THE BONDED INTERFACE SUBJECTED TO FREEZE/THAW ENVIRONMENT AND MODE I FRACTURE/FATIGUE UTILIZING THE SP3 SURFACE PROFILE

ABSTRACT

The SCCB testing methodology was utilized to ascertain the ability of the SP 3 surface profile to withstand the adverse affects from freezing and thawing is commonly referred to as durability performance. The purpose of this study is to submit the bonded interface to a calcium chloride attack while the specimen resides in a freeze/thaw environment. The treated specimen was then subjected to Mode I fatigue and fracture to ascertain the reduction in bond strength in order to quantify the bond's durability. The fracture results of the weathered specimens show that the interface region behaves in a much more brittle manner than the pristine specimens and the critical strain energy release rates achieved fifty percent of the baseline values. The variability of the weathering and SP 3 surface profile produced mix results.

KEYWORDS: concrete repair; concrete strengthening; fiber reinforced polymer; modified Paris law; fatigue

B.1 Introduction

The ability of concrete to withstand the adverse affects from freezing and thawing is commonly referred to as durability performance. The concept of concrete durability began in 1940 when the Portland Cement Association (PCA) initiated research on multiple areas of concrete durability (Mohammed, et al., 2000). The purpose of this study is to submit the bonded interface to a calcium chloride attack while the specimen resides in a freeze/thaw environment. The treated specimen will then be subjected to Mode I fatigue and fracture to ascertain the reduction in bond strength in order to quantify the bond's durability.

The calcium chloride solution was selected to replicate the effects of deicing salts that have been used for a number of years to treat iced roadways and bridges. According to Boyajian (2002), deicing salts contribute to the freeze/thaw attack in the following ways:

- By providing moisture from the melting of ice and snow in freezing weather.
- By causing additional freezing through the lowering of temperature in the subsurface zone.
- By creating a system which develops osmotic pressures.
- By a buildup of salt crystals in subsurface voids.

According to Cordon (1967), concrete is at its most vulnerable state when the internal moisture reaches the saturation point. To insure that this is achieved, the concrete must experience a head of water prior to freezing which can be easily accomplished by simply submerging the specimen in the calcium chloride solution during the freeze/thaw cycling. As the concrete specimen freezes, the water that has filled the concrete pores and voids expands. When the expansion reaches the tensile capacity of

the concrete, the concrete begins to deteriorate in the form of cracking, scaling (spalling), and crumbling.

As freezing and thawing of reinforced concrete represents an adverse environment, it is expected that there will be a reduction in fracture capacity and in fatigue capacity with each cycle duration. Boyajian (2002) and Kodkani (2004) reported significant decreases in fracture capacity of weathered specimens as well as significant (9 percent) increases in volume and weight. Furthermore, as illustrated by Abanilla et al., (2005) the epoxy should also experience a reduction in performance due to the exposure of moisture which causes plasticization, hydrolysis and epoxy deterioration.

In order to quantify the behavior of the weathered CFRP-concrete bond, the following is proposed:

1. Fracture 100 cycle, 200 cycle, and 300 cycle specimens. The methodology for these tests is identical to the process described in Chapter 2 of this work. The results will be compared to the pristine specimen results obtained previously and should allow for the quantification of bond degradation.
2. Fatigue 100 cycle, 200 cycle, and 300 cycle specimens. The methodology for these tests is identical to the process described in Chapter 4 of this work. The results will be compared to the pristine specimen results obtained previously and should allow for the quantification of bond degradation.
3. If possible, develop the modified Paris Law for weathered specimens.

B.2 Materials

The single cantilever contoured beam (SCCB) used for this study is comprised of a substrate material (reinforced concrete), a fiber reinforced polymer layer and a wood contour as illustrated in Figure B.1. The SCCB used in this study is representative of the SCCB used by Boyajian and Lawrence (2006) in that the beam length dimension is equivalent. The substrate was normal weight concrete with a target compressive strength of 41.4 MPa. The contour material used in the study is a wood product, 1.9E Microllam® LVL (Laminated Veneer Lumber) manufactured by Weyerhaeuser. Additionally, the FRP system selected for the study was Sikadur® 301 two-part epoxy and SikaWrap® Hex 103C carbon fiber due to the system's increasing popularity in industry.

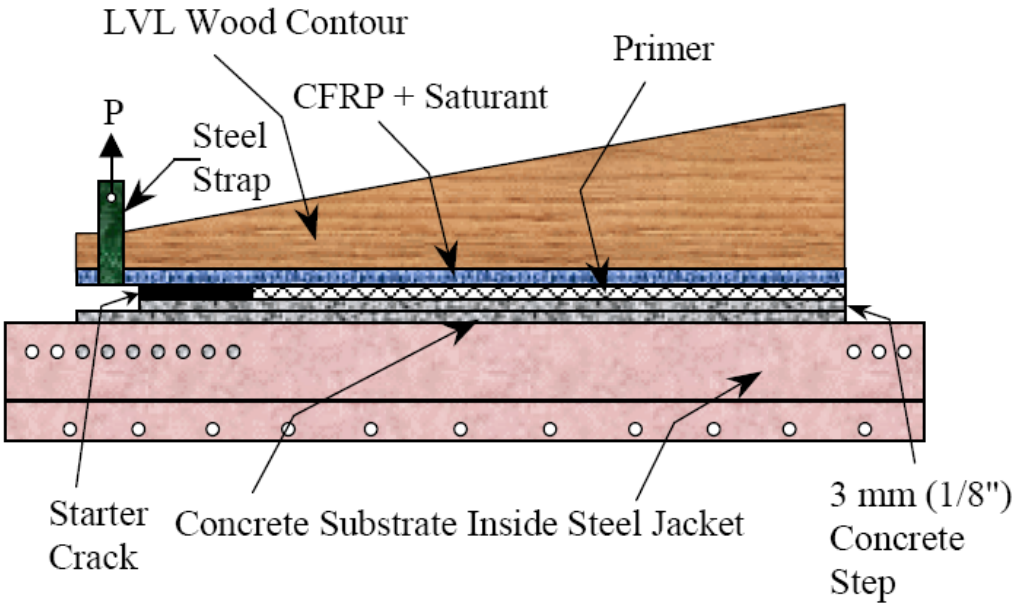

Figure B.1. Side View of Single Contoured Cantilever Beam Test (Boyajian, 2002)

B.3 Freeze/Thaw Testing Methodology

There are currently no testing standards available for concrete-FRP freeze/thaw conditioning subjected to a chloride solution. So as to be consistent with previous studies, this work will utilize the procedure put forth by Boyajian (2002) and also utilized by Davalos et al. (2008). The procedure developed by Boyajian combined ASTM C672 ("Standard Test Method for Scaling Resistance of Concrete Surfaces Exposed to Deicing Chemicals," 1998) and ASTM C666 ("Standard Test Method for Resistance of Concrete to Rapid Freezing and Thawing," 1997) to develop the testing protocol.

The freeze/thaw cycle tests required the use of 27 CFRP-Concrete specimens; 18 freeze-thaw specimens and nine baseline companion specimens. The specimens were divided evenly (six each) among the test durations of 100 cycles, 200 cycles and 300 cycle tests. For each test duration, six specimens would be subjected to freeze/thaw cycles and three would be untreated for baseline data. The CFRP-concrete specimens were placed (in an inverted position) into 76 mm deep containers and placed into an environmental chamber. The container was filled halfway with a calcium chloride solution, in accordance with ASTM C672 (1998), consisting of 4 g of dissolved calcium chloride in 100 ml of water. The specimens were then cycled in accordance to the freeze/thaw regimen provided in Figure B.2.

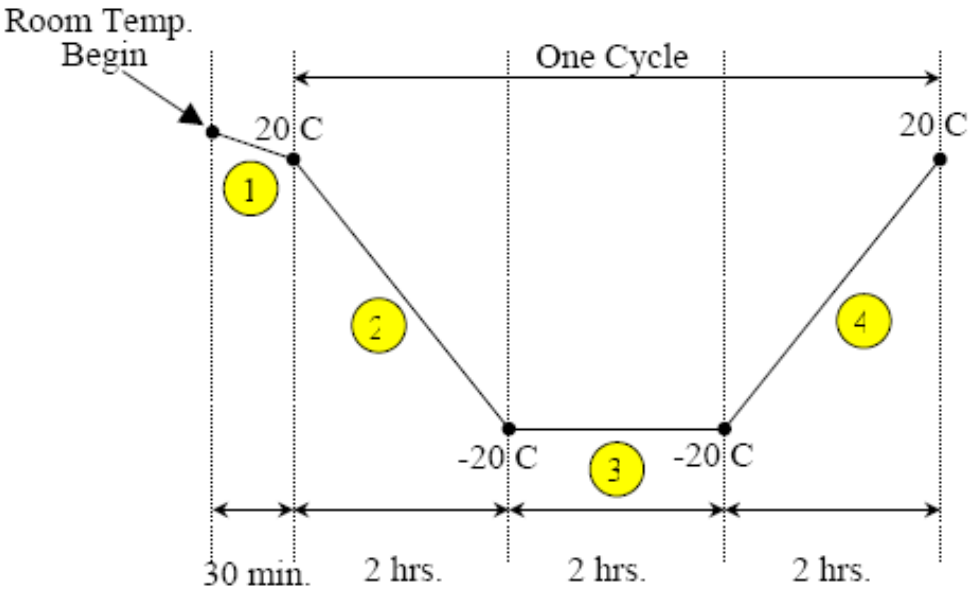

Figure B.2 Freezing and Thawing Cycle (Boyajian, 2002)

For the current study, the freeze/thaw cycles were completed for the 100, 200 and 300 cycle durations. Figure B.3 illustrates the visible changes between a pristine specimen compared to the 200 cycle and 300 cycle specimens. The 200 cycle specimens experienced considerable damage due to the testing regimen mainly in the form of crumbling. The 300 cycle specimens were severely damaged, however, as the results will show, still able to be tested by Mode I fatigue and fracture.

Figure B.3 Freeze/Thaw Specimens: 300 Cycles (left), 200 Cycles (center), and Pristine (right)

B.4 Fracture/Fatigue Testing Methodology

Fracture Test Methodology

The SCCB previously described in the materials section of this study was used to investigate the fracture behavior of the SP 3 bond interface subjected to varying levels of weathering. The SCCB specimens were placed in the Instron 5582® machine and loaded until complete interface fracture ensued. The testing regimen, as it pertains to fracture,

was consistent with those of previous studies previously presented by Boyajian (2002), Lawrence and Boyajian (2006).

Fatigue Test Methodology

For the foundational work of fatigue of the weathered bonded interface using the SCCB, twelve SCCB specimens will be used to determine the behavior of the bond. Furthermore, if possible, the fatigue data will be used to develop the modified Paris Law. In an effort to stay consistent with the pristine fatigue study, a frequency of five hertz was selected as the cyclic rate. Additionally, it is the authors' opinion that load ratio will have an effect on the fatigue life of the bonded interface and therefore $R = 0.5$, was selected to provide mid level values (e.g. R: $0 \rightarrow 1$) for the current study. The testing regimen, as it pertains to fatigue, consisted of placing the SCCB specimens in the 20-Kip MTS® machine and submitting them to the described cyclic loading until interface failure was achieved.

B.5 Fracture Test Results

As pointed out by Karbhari et al. (2000), the durability of the system depends on the weathering damage to three separate entities: (1) the response of the concrete substrate to weathering; (2) the response of the CFRP to weathering; and (3) the response of the concrete-CFRP bonded region.

The fracture test results met expectations in that the specimens exhibited a considerable reduction in strain energy release rates which was also experience in previous studies of Boyajian (2002) and Kodkani (2004). It should be noted, however, for all cycles (100-300) that the plane of failure did note penetrate the substrate as deeply as with the pristine specimens, but was still located in the substrate. Clearly this would

indicate damage to the interface region as a result of weathering. As illustrated by Figure B.4, the interface failure has moved closer towards the CFRP layer or in other words moved up through the interface region. A close up photo of the failed interface region is given in Figure B.5.

Figure B.4. Fracture of the Concrete to CFRP Interface Region – 300 Freeze/Thaw Cycles

For the 100 cycle fractured specimen, the critical load, Pc was found to be 622 N. This represented a reduction of 53 percent in the critical load. The critical strain energy curve for the 100 cycle specimen is illustrated in Figure B.6.

Figure B.5. Close up of Fractured Interface Region – 200 Freeze/Thaw Cycles

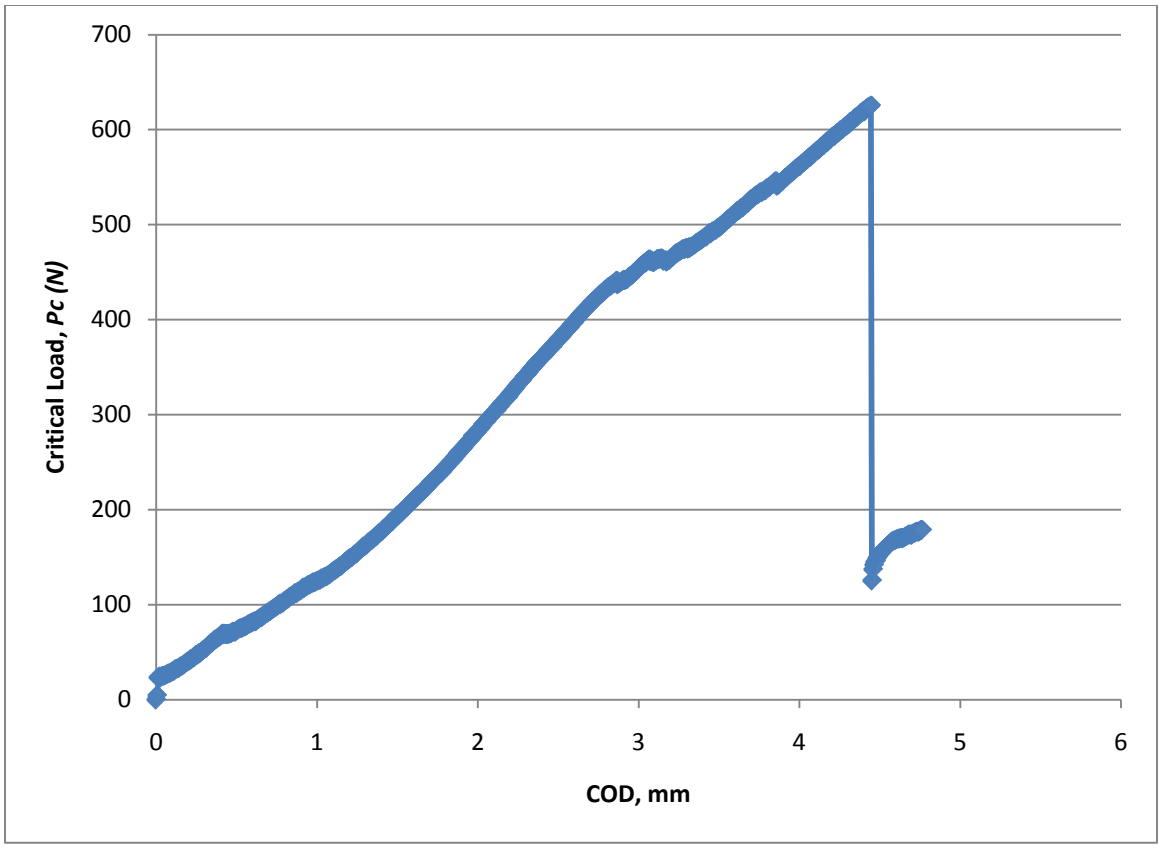

Figure B.6 Fracture Energy – 100 Freeze/Thaw Cycles

For the 200 cycle fractured specimen, the critical load, Pc was found to be 622 N . This represented a reduction of 58 percent in the critical load. The critical strain energy curve for the 200 cycle specimen is illustrated in Figure B.7.

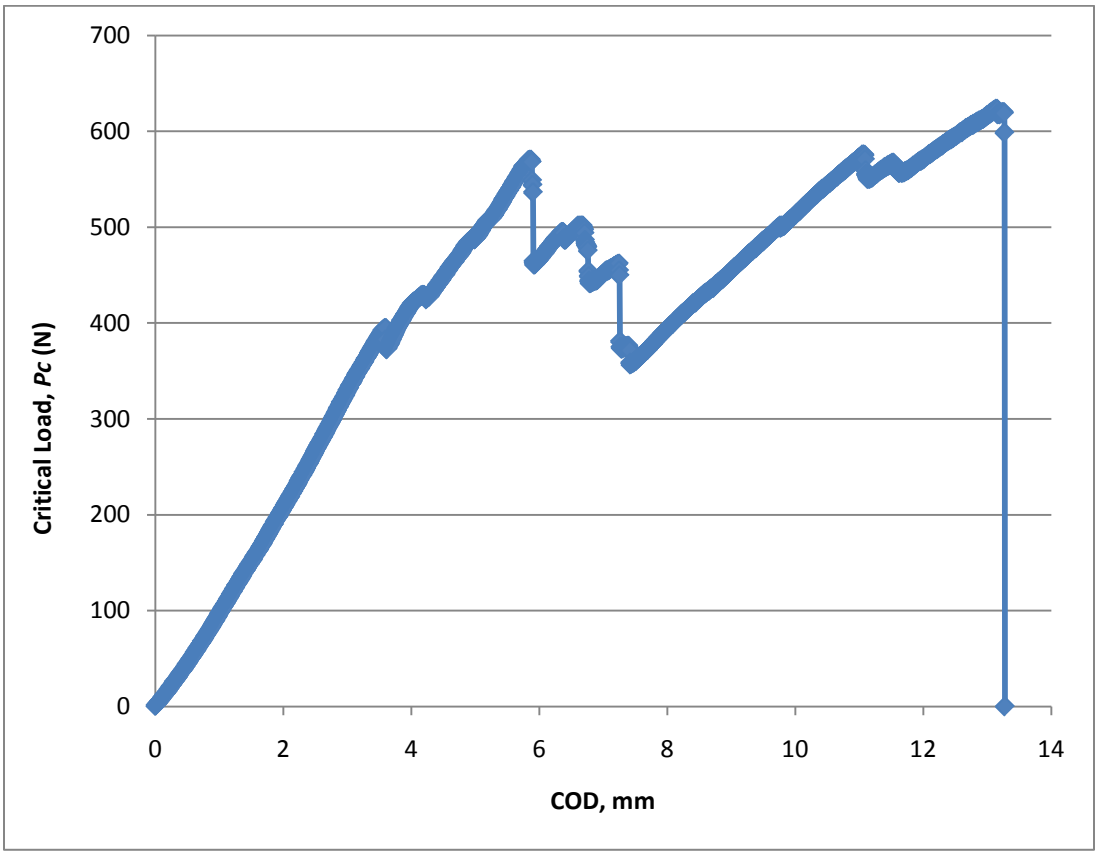

Figure B.7 Fracture Energy – 200 Freeze/Thaw Cycles

For the 300 cycle fractured specimen, the critical load, *Pc* was found to be 578 N. This represented a reduction of 61 percent in the critical load. The critical strain energy curve for the 300 cycle specimen is illustrated in Figure B.8.

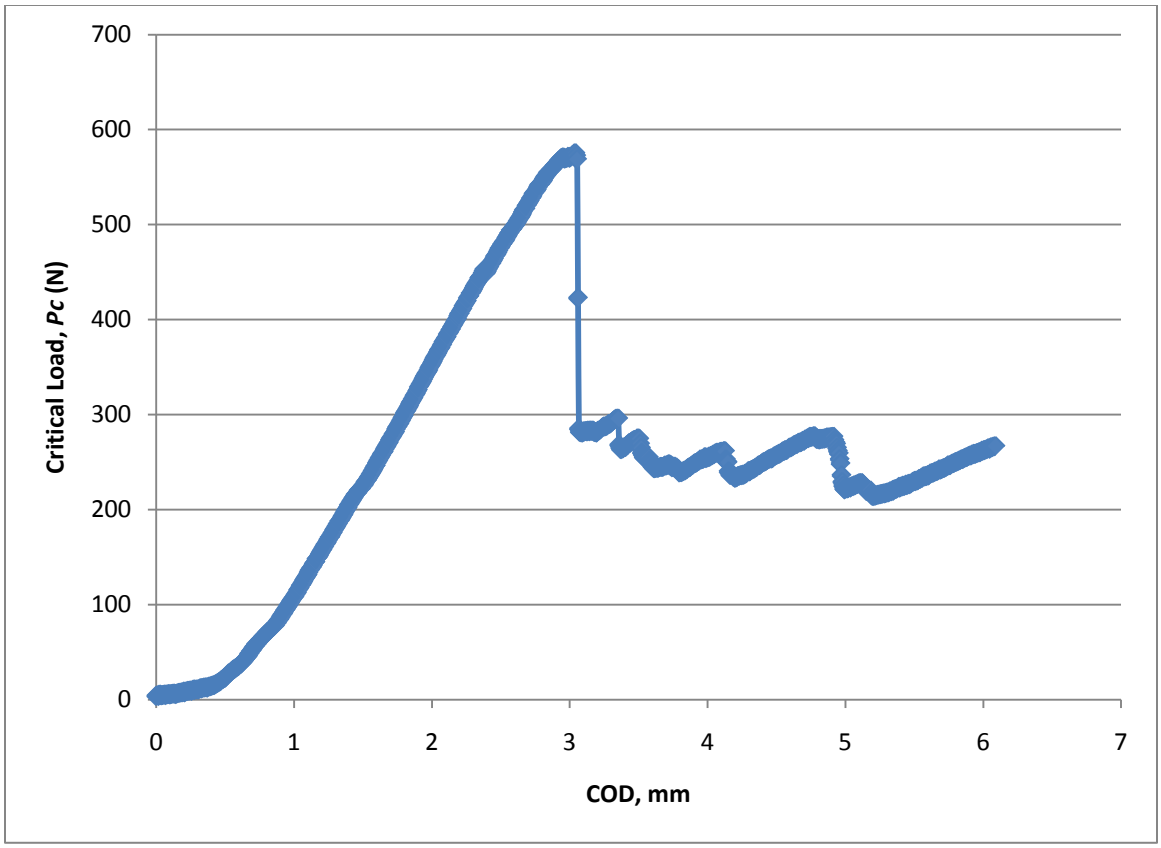

Figure B.8 Fracture Energy – 300 Freeze/Thaw Cycles

B.6 Discussion – Fatigue Testing Results

The fatigue testing yielded mixed results in that most specimens never achieved failure or failed in so few cycles that they were considered to be fractured. This phenomenon was at first attributed to the ability to determine the applied load that would ultimately lead to failure. The pristine studies utilized 80 percent of the fracture critical load with good success. For example, the initial fatigue load for the 300 freeze/thaw cycle specimens was determined to be 80 percent of 578 N or 436 N. However, for the weathered specimens, this approach was clearly unable to achieve the level of success needed to develop the modified Paris Law for fatigue life. The test results are listed in Table B.1. The specimen labeling system represents whether the specimen was

weathered, the number of freeze/thaw cycles, the date of the concrete pour, and the order of testing for fatigue. For example, FT200_711_01 would represent a freeze/thaw specimen that was subjected to 200 cycles of freezing and thawing, the concrete pour occurred on July 11th and it was the first specimen tested. Table B.1 organizes the test result based on whether the specimen failed due to fatigue, fracture, run-out (exceed 10 million cycles) or was not tested due to bond failure and three were saved for future testing.

Table B.1. Weathered Specimen Results – Cyclic Loading

Freeze/Thaw Cycles	Total	Fatigue	Fracture	Run-Out (10 million cycles)	Not Tested
100 Cycles	**6**				
FT100_7/11_01			X		
FT100_7/11_02				X	
FT100_7/11_03				X	
FT100_7/11_04					X
FT100_7/11_05					X
FT100_7/11_06					X
200 Cycles	**6**				
FT200_7/11_01			X		
FT200_7/11_02				X	
FT200_7/11_03				X	
FT200_7/11_04				X	
FT200_7/11_05		X			
FT200_7/11_06					X
300 Cycles	**6**				
FT300_10/30_01					X
FT300_10/30_02					X
FT300_10/30_03			X		
FT300_10/30_04			X		
FT300_10/30_05				X	
FT300_10/30_06				X	
TOTALS	**18**	**1**	**4**	**7**	**6**

As can be seen in the table, four specimens fractured, seven specimens exceed 10 million cycles and only one failed due to fatigue. The crack opening displacement verses number of cycles graph for the fatigue specimen is given by Figure B.9 while the failed specimen is illustrated in Figure B.10.

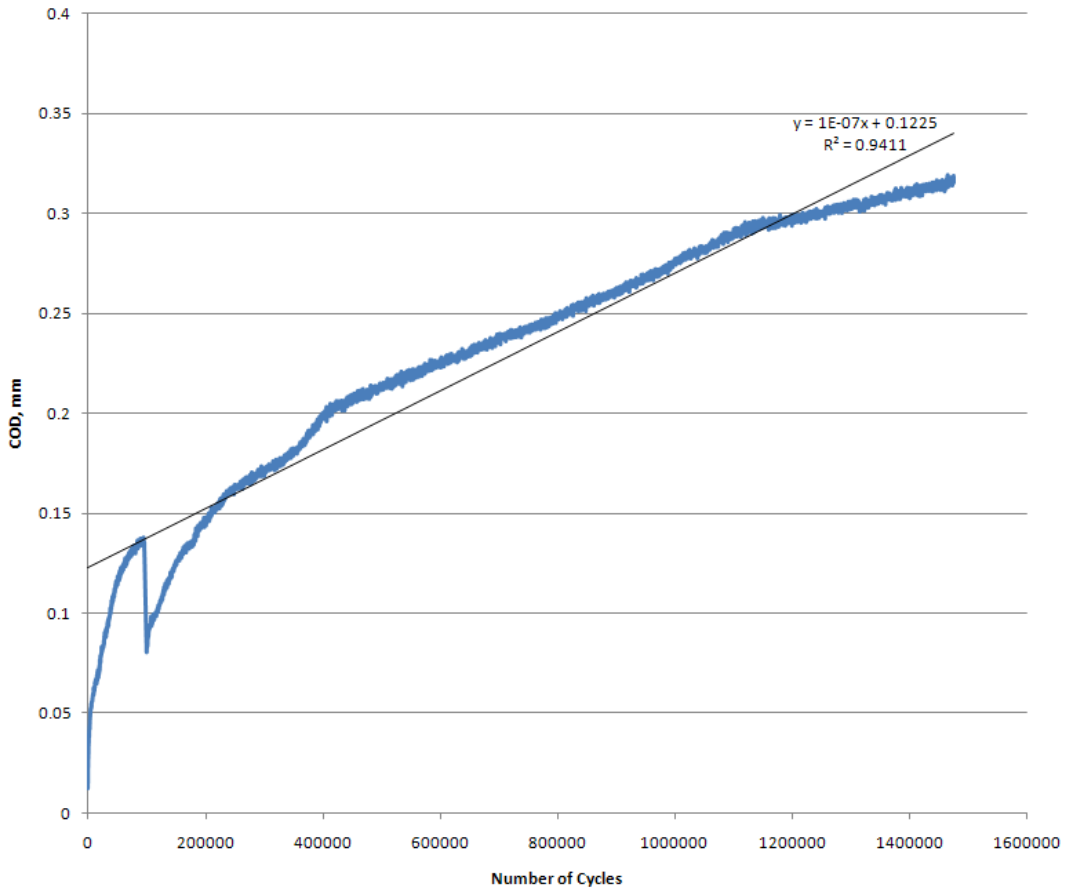

Figure B.9 COD Versus Number of Cycles for a SCCB Specimen Under 267-534 N Cyclic Loading with a Frequency f = 5 Hz, Load Ratio R = 0.5 and Sinusoidal Waveform

Six specimens were not tested; three due to pre-test interface failure and three were saved for future testing. The 200 and 300 cycle specimens (three in total) were not

tested due to interface failure before testing could commence. An example of the pre-test failure is illustrated in Figure B.11. The cause of the interface failure is due to a material

Figure B.10 Fatigue Failure – 200 Freeze/Thaw Cycles

Figure B.11 Pre-Test Failure of the CFRP to Concrete Interface – 300 Freeze/Thaw Cycles

change in the Microllam® LVL. The newer product is more porous than the previous LVL used in the study. This caused the LVL to more readily absorb the epoxy and then warp upon curing. The warping provided enough energy to fracture the interface of these specimens. In an effort to reduce the amount of absorption, the virgin wood was pretreated with either epoxy or a wood sealer. Figure B.12 illustrates the absorption of epoxy for the epoxy pretreatment (top), virgin surface (middle), and wood sealer pretreatment (bottom). As illustrated by the figure, all pretreatments still experienced significant absorption and after curing, the wood contours continued to warp. Finally, the newer Microllam® LVL was abandoned for the Microllam® LVL utilized in the previous study.

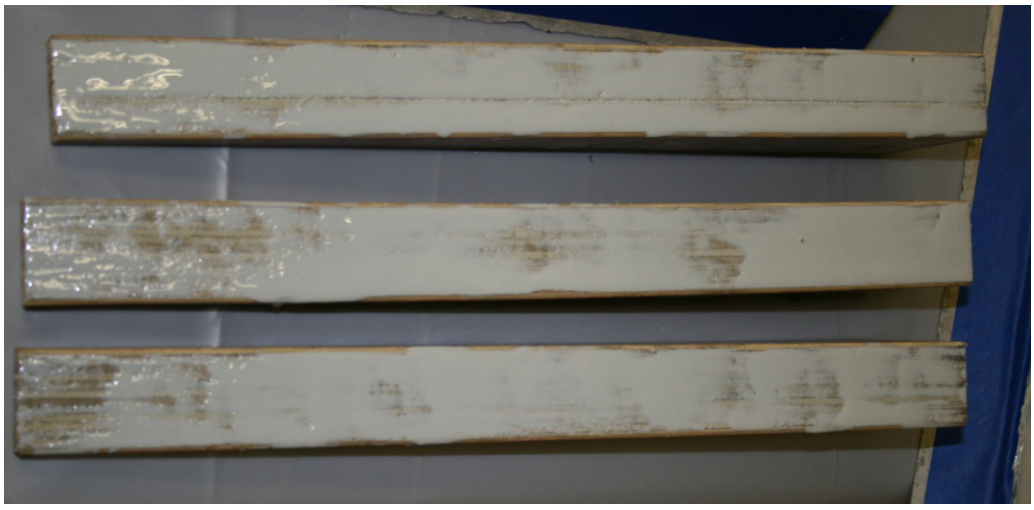

Figure B.12 Absorption of Epoxy by Microllam® LVL

B.7 Conclusions and Future Directions

The fracture results of the weathered specimens show that the interface region behaves in a much more brittle manner than the pristine specimens of the earlier study

which was expected due to the findings of Shahrooz et al. (2003). In the Shahrooz study, it was determined that CFRP fabrics/epoxy systems became brittle during the freeze-thaw cycling period.

Of further importance is the location of the fracture plane for the weathered specimens. As previously stated, the wet conditions of freeze/thaw (Abanilla et al., 2005) should result in some degradation of the epoxy. However, while the failure was shallower in nature, e.g. closer to the bonded area than with the pristine specimens, the epoxy bond proved to still be stronger than the damaged concrete. The result of the material failure is still a cohesive failure instead of the expected adhesive failure reported by Davalos et al. (2008) and Boyajian (2002).

The behavior of the SP 3 surface profile is inconsistent as it pertains to durability testing of fatigue. The number of run-out tests suggests that the critical fatigue load is not being achieved. As a way to better define the critical fatigue load, a sample run-out specimen was fractured to determine exactly what was causing the inconsistencies. Using specimen FT300_1030_04, a critical strain energy fracture test was performed and the results are presented in Figure B.13.

It should be noted, that the specimen, FT300_1030_04 was subjected to 10 million loading cycles with no crack propagation before it was fractured. Clearly, the critical load of 823 N is much larger than the previous fractured specimen that only achieved 578 N. Upon inspection of the failed interface, Figure B.14 and B.15, the crack propagated primarily in the weathered concrete, although, the failure did occur shallower than the pristine specimens. This would suggest that the variability of the critical load is a function of the weathered interface.

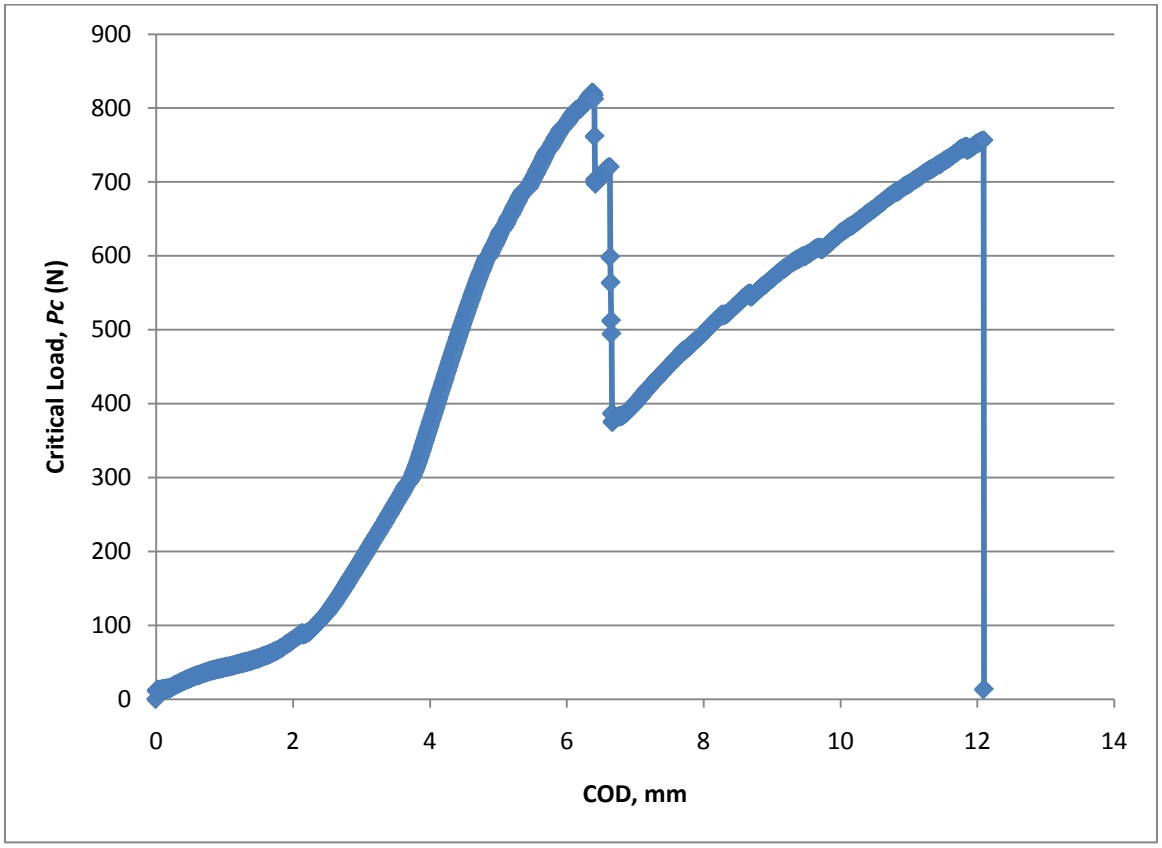

Figure B.13 Fracture Energy of Run-out Specimen – 300 Freeze/Thaw Cycles

Figure B.14 Failed Interface Region of Run-out Specimen – 300 Freeze/Thaw Cycles

Figure B.15 Close up of Fractured Interface Region – 300 Freeze/Thaw Cycles

The current study both answered questions and raised questions. The following summarizes the future direction of research.

1. The damage caused by the weathering cycles needs to be quantified for each cycle duration. As of now, the variability of critical load from one specimen to the next is too high to develop the modified Paris Law. This could be accomplished through a microscopic analysis of the failed interface region and possibly peel tests.
2. The newer Microllam® LVL, while a fine product, cannot be utilized for the SCCB. This would pose a problem for future studies given that the original Microllam® LVL is no longer available. The use of Plexiglas should be studied as a viable alternative for the SCCB testing system.

3. The SP 3 surface profile still produced a bond that was stronger than the interface causing material failure and not bond failure. However, it is hypothesized that the SP 3 surface profile produces an inconsistent surface at the micro-level and is a driving factor in the variability of the fatigue results. This should be studied further by varying the surface preparation and then subjecting the specimens to freeze-thaw cycling.

APPENDIX C: SAMPLE FINITE ELEMENT ANALYSIS INPUT FILE

The following is a sample input file of the single contour cantilever beam. The abbreviation is required due to the size of the input file. *A full input file can be requested by the written permission of the author*.

```
*Heading
** Job name: Final_v3 Model name: Model-1
*Preprint, echo=NO, model=NO, history=NO, contact=NO
**
** PARTS
**
*Part, name=Part-1
*Elset, elset=_PickedSet174, internal, generate
 2133,  2232,     1
** Section: FRP
*Solid Section, elset=_PickedSet50, material=FRP
1.7,
** Section: Cohesive
*Cohesive Section, elset=_PickedSet173, controls=EC-1, material=Cohesive,
response=TRACTION SEPARATION
, 1.7
** Section: Wood
*Solid Section, elset=_PickedSet49, material=Wood
1.7,
** Section: Section-1
*Solid Section, elset=_PickedSet54, material=Concrete
1.7,
** Section: Section-1
*Solid Section, elset=_PickedSet174, material=Concrete
1.7,
** Section: Section-1
*Solid Section, elset=_PickedSet77, material=Concrete
1.7,
*End Part
**
**
** ASSEMBLY
**
*Assembly, name=Assembly
**
*Instance, name=Part-1-1, part=Part-1
*End Instance
```

```
**
*Nset, nset=_PickedSet15, internal, instance=Part-1-1
  12,  15,  22, 697, 698, 699, 700, 701, 702, 703, 704, 705, 706, 707, 708, 709
 710, 711, 712, 713, 714, 715, 716, 717, 718, 719, 720, 721, 722, 723, 724, 725
 726, 727, 728, 729, 730, 731, 732, 733, 734, 735, 736, 737, 738, 739, 740, 741
 742, 743, 744, 745, 746, 747, 748, 749, 750, 751, 752, 753, 754, 755, 756, 757
 758, 759, 760, 761, 762, 763, 764, 765, 766, 767, 768, 769, 770, 771, 772, 773
 774, 775, 776, 777, 778, 779, 780, 781, 782, 783, 784, 785, 786, 787, 788, 789
 790, 791, 792, 793, 794, 795, 1041, 1042, 1043, 1044, 1045, 1046, 1047, 1048, 1049,
1050
 1051, 1052, 1053, 1054, 1055, 1056, 1057, 1058, 1059, 1060, 1061, 1062, 1063, 1064,
1065, 1066
 1067, 1068, 1069, 1070, 1071, 1072, 1073, 1074, 1075, 1076, 1077, 1078, 1079, 1080,
1081, 1082
 1083, 1084, 1085, 1086, 1087, 1088, 1089
*Elset, elset=_PickedSet15, internal, instance=Part-1-1
 813, 819, 825, 831, 837, 843, 849, 855, 861, 867, 873, 879, 885, 891, 897, 903
 909, 915, 921, 927, 933, 939, 945, 951, 957, 963, 969, 975, 981, 987, 993, 999
 1005, 1011, 1017, 1023, 1029, 1035, 1041, 1047, 1053, 1059, 1065, 1071, 1077, 1083,
1089, 1095
 1101, 1107, 1113, 1119, 1125, 1131, 1137, 1143, 1149, 1155, 1161, 1167, 1173, 1179,
1185, 1191
 1197, 1203, 1209, 1215, 1221, 1227, 1233, 1239, 1245, 1251, 1257, 1263, 1269, 1275,
1281, 1287
 1293, 1299, 1305, 1311, 1317, 1323, 1329, 1335, 1341, 1347, 1353, 1359, 1365, 1371,
1377, 1383
 1389, 1395, 1401, 1407, 3761, 3767, 3773, 3779, 3785, 3791, 3797, 3803, 3809, 3815,
3821, 3827
 3833, 3839, 3845, 3851, 3857, 3863, 3869, 3875, 3881, 3887, 3893, 3899, 3905, 3911,
3917, 3923
 3929, 3935, 3941, 3947, 3953, 3959, 3965, 3971, 3977, 3983, 3989, 3995, 4001, 4007,
4013, 4019
 4025, 4031, 4037, 4043, 4049, 4055
*Nset, nset=_PickedSet18, internal, instance=Part-1-1
 21,
*Nset, nset=_PickedSet22, internal, instance=Part-1-1
 21,
*Nset, nset=_PickedSet23, internal, instance=Part-1-1
 8,
*Nset, nset=_PickedSet24, internal, instance=Part-1-1
 11,
*End Assembly
**
** ELEMENT CONTROLS
**
```

```
*Section Controls, name=EC-1, ELEMENT DELETION=YES, MAX
DEGRADATION=0.95, VISCOSITY=0.001
1., 1., 1.
*Amplitude, name=Amp-1, time=TOTAL TIME, definition=SMOOTH STEP
0., 0., 120., 1.
**
** MATERIALS
**
*Material, name=Cohesive
*Damage Initiation, criterion=QUADS
2250.,15000.,15000.
*Damage Evolution, type=ENERGY, power=1.
 0.85,
*Elastic, type=TRACTION
 1.45046e+08, 1.45046e+08, 1.45046e+08
*Material, name=Concrete
*Elastic
 4.4152e+06, 0.18
*Material, name=FRP
*Elastic
 4.9e+06, 0.18
*Material, name=Wood
*Elastic
 1.2e+06, 0.3
**
** BOUNDARY CONDITIONS
**
** Name: BC-1 Type: Displacement/Rotation
*Boundary
_PickedSet15, 1, 1
_PickedSet15, 2, 2
_PickedSet15, 6, 6
** Name: BC-4 Type: Displacement/Rotation
*Boundary
_PickedSet23, 1, 1
_PickedSet23, 2, 2
** Name: BC-5 Type: Displacement/Rotation
*Boundary
_PickedSet24, 1, 1
_PickedSet24, 2, 2
** ----------------------------------------------------------------
**
** STEP: Step-1
**
*Step, name=Step-1, nlgeom=YES, inc=1000
*Static
```

```
0.001, 1., 1e-08, 1.
**
** BOUNDARY CONDITIONS
**
** Name: BC-3 Type: Displacement/Rotation
*Boundary
_PickedSet22, 2, 2, 0.07
**
** OUTPUT REQUESTS
**
*Restart, write, frequency=0
**
** FIELD OUTPUT: F-Output-1
**
*Output, field
*Node Output
CF, RF, U
*Element Output, directions=YES
LE, PE, PEEQ, PEMAG, S, SDEG, STATUS
*Contact Output
CDISP, CSTRESS
**
** HISTORY OUTPUT: H-Output-1
**
*Output, history, variable=PRESELECT *End Step
```

APPENDIX D: MISCELLANEOUS SPECIMEN PHOTOS

The following represents a sample photos taken during the testing for this study. Other photos of the process is available with the written permission of the author.

Specimen Construction

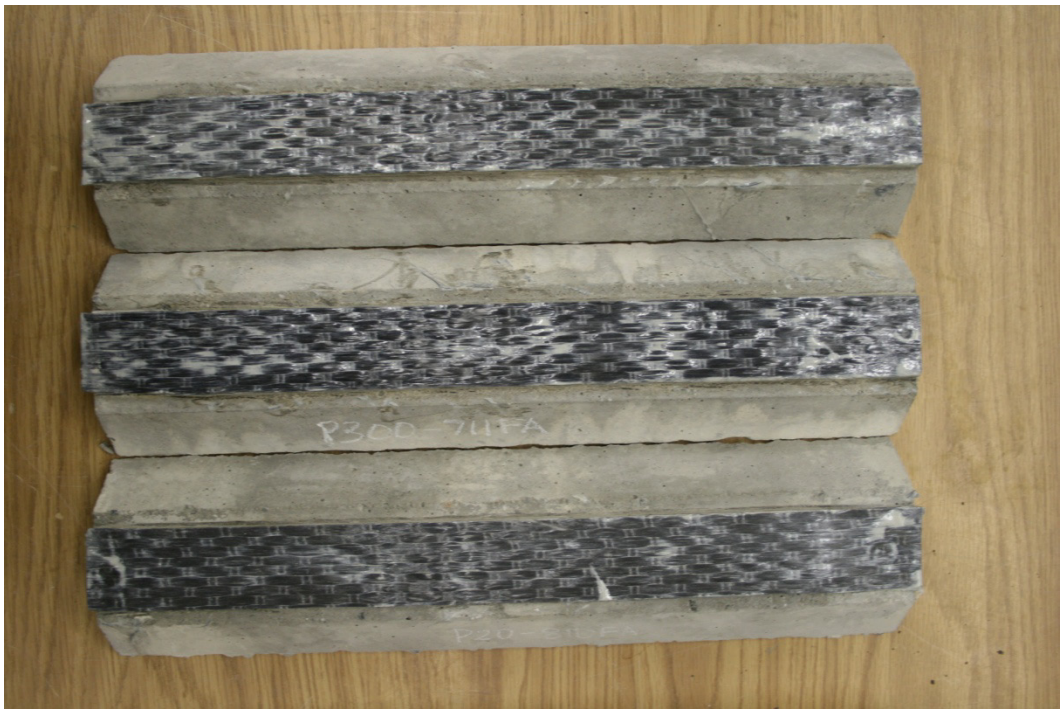

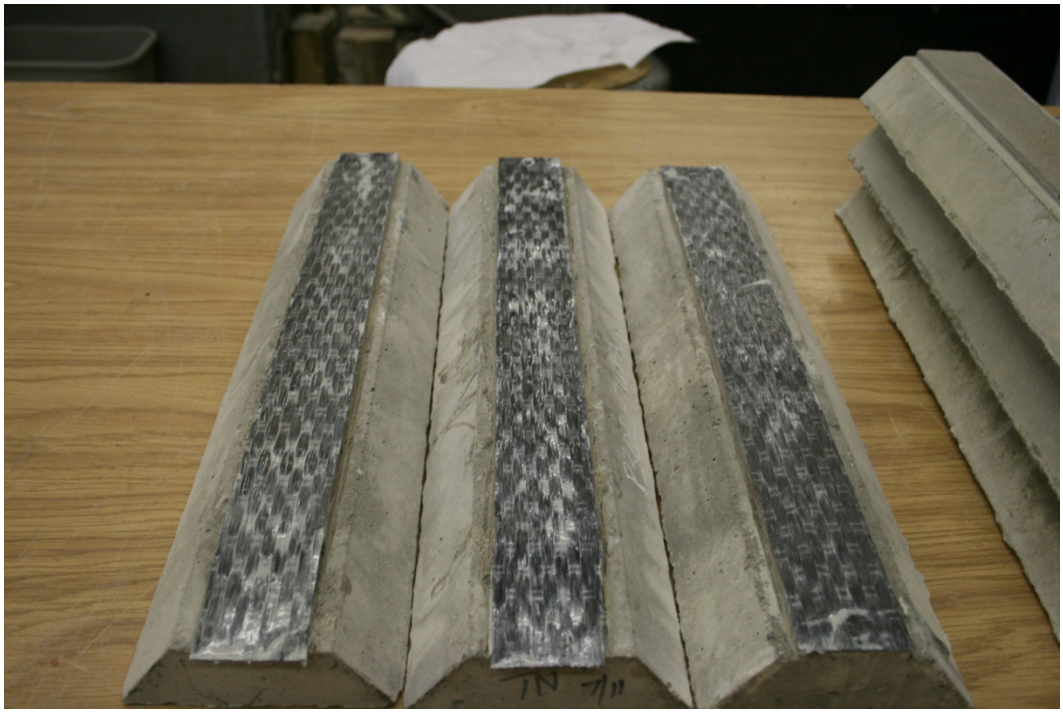

Failed in Fatigue

Failed in Pre-Cracking

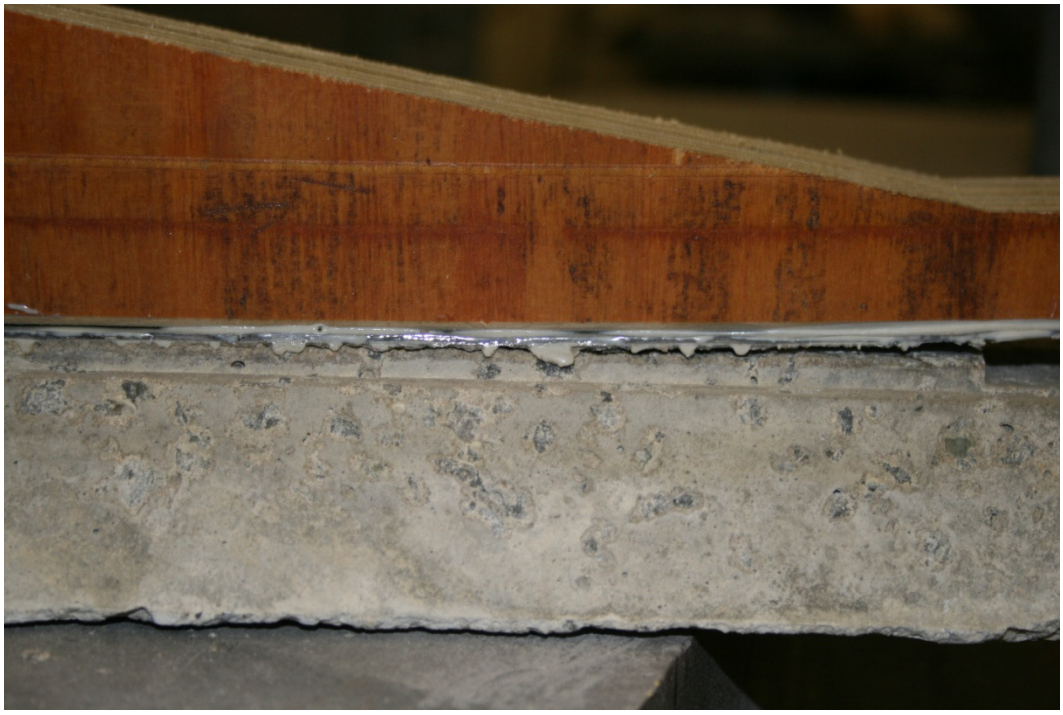

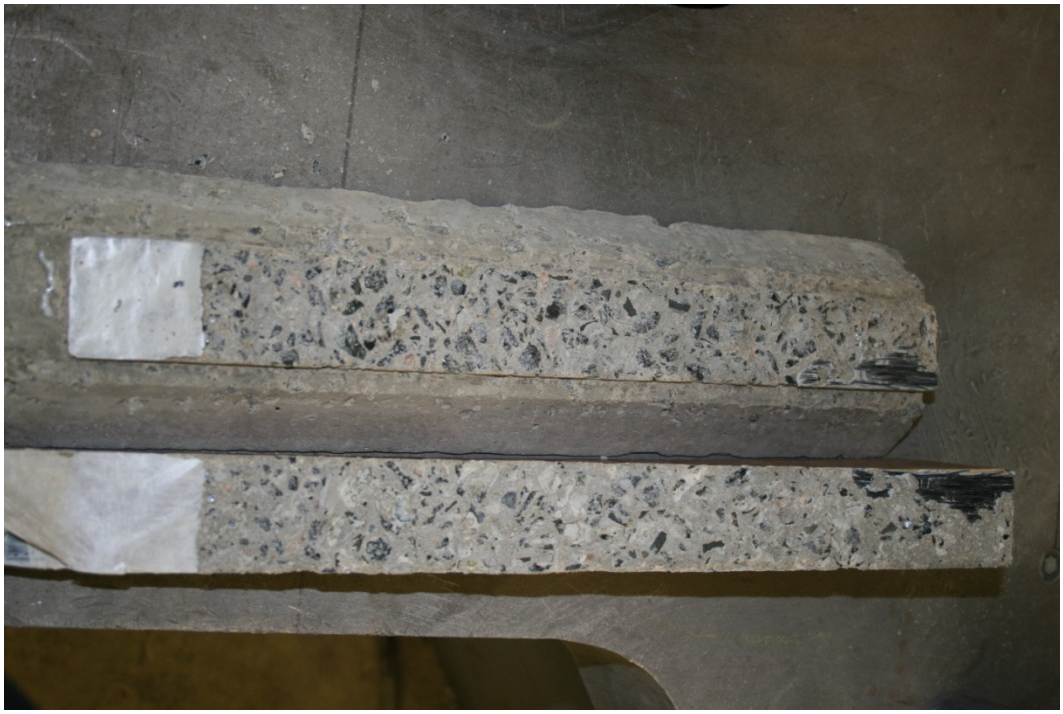

Weathered Fracture